ESPOO 2006 VTT PUBLICATIONS 598

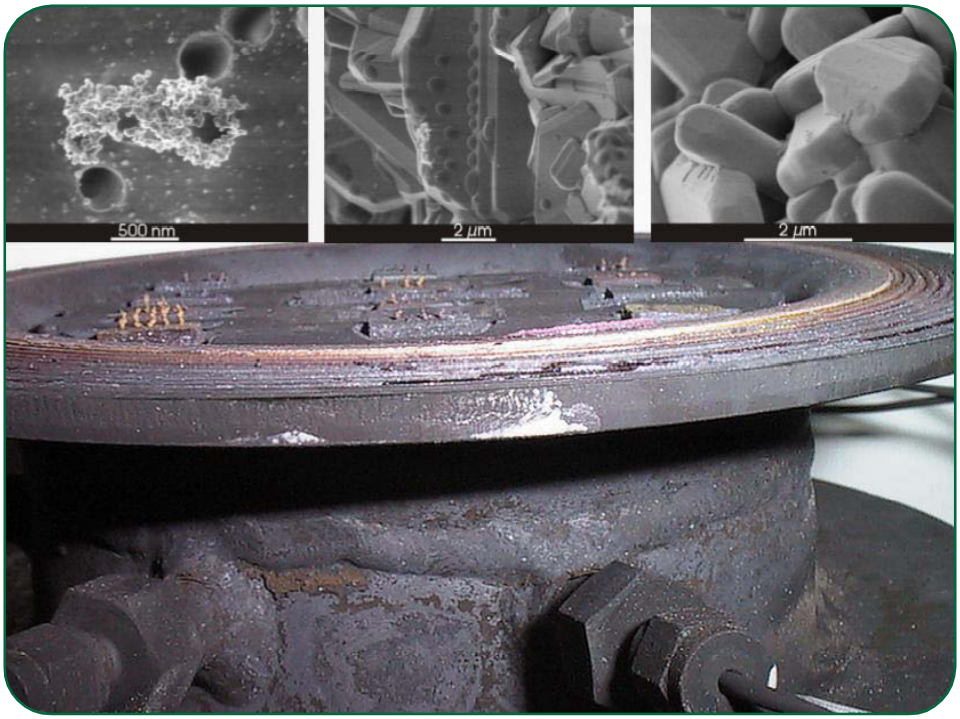

Jussi Lyyränen

Particle formation, deposition, and particle induced corrosion in large-scale medium-speed diesel engines

VTT PUBLICATIONS 598

Particle formation, deposition, and particle induced corrosion in large-scale medium-speed diesel engines

Jussi Lyyränen

Dissertation for the degree of Doctor of Science in Technology to be presented with due permission for public examination and debate in Auditorium Ke2 at Helsinki University of Technology (Espoo, Finland) on the 28th of April, 2006 at 12 o'clock noon.

ISBN 951–38–6708–0 (soft back ed.)
ISSN 1235–0621 (soft back ed.)

ISBN 951–38–6831–1 (URL: http://www.vtt.fi/inf/pdf/)
ISSN 1455–0849 (URL: http://www.vtt.fi/inf/pdf/)

JULKAISIJA – UTGIVARE – PUBLISHER

VTT, Vuorimiehentie 3, PL 1000, 02044 VTT
puh. vaihde 020 722 111, faksi 020 722 4374

VTT, Bergsmansvägen 3, PB 1000, 02044 VTT
tel. växel 020 722 111, fax 020 722 4374

VTT Technical Research Centre of Finland, Vuorimiehentie 3, P.O.Box 1000, FI-02044 VTT, Finland
phone internat. +358 20 722 111, fax + 358 20 722 4374

VTT, Biologinkuja 7, PL 1000, 02044 VTT
puh. vaihde 020 722 111, faksi 020 722 7021

VTT, Biologgränden 7, PB 1000, 02044 VTT
tel. växel 020 722 111, fax 020 722 7021

VTT Technical Research Centre of Finland, Biologinkuja 7, P.O. Box 1000, FI-02044 VTT, Finland
phone internat. +358 20 722 111, fax +358 20 722 7021

Technical editing Anni Kääriäinen

Otamedia Oy, Espoo 2006

Lyyränen, Jussi. Particle formation, deposition, and particle induced corrosion in large-scale medium-speed diesel engines [Hiukkasten muodostuminen, depositio ja hiukkasten aiheuttama korroosio suurissa, keskinopeissa dieselmoottoreissa]. Espoo 2006. VTT Publications 598. 72 p. + app. 123 p.

Keywords particles, particle formation, particle emissions, deposition, corrosion, internal combustion engines, medium-speed diesel engines, large-scale diesel engines, particle characteristics, laboratory-scale studies

Abstract

The objective of this work was to study the formation of particles and their morphology and chemical composition in large-scale diesel engines operating with low-grade residual fuel oils. The effect of a Mg-based fuel oil additive on exhaust gas particles was also investigated. Particle characteristics were determined by means of the methods of aerosol technology, chemical analyses, and electron microscopy. As particle and deposit formation and characteristics play an important role in corrosion and erosion, the particle characterisation studies provided the necessary background information.

The mass size distributions from the large-scale diesel engines were bimodal, with a main ("small") mode at 60–90 nm and a "large" mode at 7–10 μm. The small mode particles were formed by the nucleation of volatilised fuel oil ash species, which grew further by condensation and agglomeration. The large-mode particles were mainly agglomerates of different sizes consisting of small particles. These particles were re-entrained from deposits and fuel residue particles of different sizes. The number size distributions peaked at 40–60 nm. Agglomerates consisting of these primary spherical particles were also found. TEM micrographs revealed that these particles consisted of even smaller structures. On the basis of the mass and elemental size distributions, evidence that the fuel oil ash was highly volatile was found. The main causes for the differences in the aerosol size distributions were the engine type and fuel oil properties.

By estimating the chemical compounds formed on the basis of ICP and EDS analyses at the corresponding mode in mass size distributions (about 0.1 μm), it was found that there was not enough oxygen in the particles to form only V_2O_5.

Complete oxidation of vanadium into vanadium pentoxide was not favourable. This can be caused by many different factors, such as short residence times or soot particles acting as surface toxicants by blocking the active surface. However, the amount of sulphuric acid in the particles was high, about 27 wt. %. This required the formation of vanadium pentoxide to catalyse the formation of SO_3 to form sulphuric acid.

Doping the heavy fuel oil with a Mg-based additive caused another mode at about 2 μm in mass size distributions, making the size distributions trimodal. The 2-μm mode was generated by magnesium, together with some vanadium, nickel, and sulphur. Particle formation was not affected by the fuel oil additive.

Deposition and corrosion studies on the surfaces of the Nimonic 80 A sample slabs were carried out on a laboratory-scale with a newly set-up deposition-corrosion apparatus (DCA). With this device the formation of the exhaust ash particles, gas composition, and deposition and corrosion on the sample slabs occurs in a similar way as in large-scale engines. Although corrosion studies have been carried out before, the formation of a corrosive ash layer when the particles deposit on the sample slabs has not previously been taken into account. Furthermore, the possible transformation of the deposited particles when they start to react to form a corrosive ash deposit has not been considered.

In the deposition and corrosion experiments with $SO_2(g)$ and synthetic ash particle feeds, almost all of the particles observed looked like flat "pools" with small spherical particles in the middle of the "pool". Condensing sulphuric acid had dissolved the particles. Small (70–90-nm) spherical particles were also observed with an $SO_2(g)$ feed. On the other hand, hardly any S was found in the deposits. This indicated that S, in the form of $SO_2(g)/SO_3(g)$, was transported through the deposit into the interface between the base material (pit area) and bottom of the deposit by molecular diffusion.

The critical issue in the propagation of corrosion was the definition of the corrosion pit depth and the thickness of the bottom layer, because the latter increased with temperature (26 μm at 700 versus 87 μm at 750°C). There was no maximum at 700°C, as in the case when considering only the depth of the corrosion pit.

A zone of “black islands” (15–33 wt. % S, the rest mainly Cr, Ni, and Ti) was found on the samples with SO_2(g) and synthetic ash particle (SAP) feeds. The composition of these islands suggested that they were composed of a “mixed”-type sulphide ((Cr, Ti, Ni)S_x). As there was hardly any O available in this bottom layer, the “black islands” were formed by internal sulphidation. However, some of these islands were different from the others, consisting of 26 wt. % Cr, 37 wt. % Ti, and 26 wt. % O, the rest being V and Ni. These islands may be the “pre-existing” form of the oxide-rich layer found in the pit. The sulphur-rich “black islands” may transform into these oxygen- and vanadium-containing islands, as more and more oxygen diffuses into the bottom reacted layer where these islands were located and as the layer in the pit area grows. Because of a strong oxygen concentration gradient existing over the formed oxide scale (pit area), and the inward diffusing SO_2/SO_3 coming into contact with the base material (metal) at the interface between the deposit base and base material, SO_2/SO_3 becomes unstable. Thus it will dissociate to form atomic sulphur and oxygen molecule, and provides the sulphur needed for the internal sulphidation reaction (i.e. the formation of “black islands”). However, based on calculations of thermodynamical stability diagrams the formation of the nickel chromates and sulphates (e.g. type II hot corrosion, also called “low temperature hot corrosion”) can not be entirely ruled out without further investigation with help of, e.g. XPS, XRD, from the corrosion pit area and bottom layer underneath it.

To verify the experimental findings, an exhaust valve from a field endurance test of 8600 h in duration was analysed. A similar zone of sulphur-containing “black islands” was observed. However, the composition of these islands differed from that of those detected in the experimental system, as they contained much more Ni (about 70–80 wt. %) and less Ti (about 5 wt. %) and S (about 5–10 wt. %). As the temperature of the valve (T = 500°C) and oxygen content of the exhaust gas were different, the results are not directly comparable. However, there can still be similarities in the basic formation mechanism of these islands. Moreover, the corrosion results (amounts) obtained with this experimental set-up are of the same order as that which has been found in large-scale diesel engines.

Lyyränen, Jussi. Particle formation, deposition, and particle induced corrosion in large-scale medium-speed diesel engines [Hiukkasten muodostuminen, depositio ja hiukkasten aiheuttama korroosio suurissa, keskinopeissa dieselmoottoreissa]. Espoo 2006. VTT Publications 598. 72 s. + liitt. 123 s.

Avainsanat particles, particle formation, particle emissions, deposition, corrosion, internal combustion engines, medium-speed diesel engines, large-scale diesel engines, particle characteristics, laboratory-scale studies

Tiivistelmä

Tässä työssä tutkittiin suurissa dieselmoottoreissa muodostuvia tuhkahiukkasia, niiden morfologiaa ja kemiallista koostumusta käytettäessä paljon tuhkaa (> 0,1 p.-%) sisältäviä jäännöspolttoaineita. Lisäksi tarkasteltiin Mg-pohjaisen lisäaineen vaikutusta tuhkahiukkasten muodostumiseen. Hiukkastutkimus loi myös välttämättömän pohjan hiukkasten deposoitumisen aiheuttamalle eroosio- ja korroosiotutkimukselle.

Suurten dieselmoottoreiden hiukkasmassakokojakaumat olivat kaksihuippuisia: päähuippu (pienet hiukkaset) oli 60–90 nm ja pieni huippu (isot hiukkaset) 7–10 µm kokoisissa hiukkasissa. Pienet hiukkaset muodostuivat polttoaineen haihtuvien tuhkaosaslajien ydintyessä, ja ne kasvoivat tiivistymällä ja liittymällä yhteen. Suuret hiukkaset koostuivat pääasiassa pienten hiukkasten muodostamista, erikokoisista yhteenliittyneistä hiukkasista. Nämä hiukkaset olivat depositioista irronneita ja/tai polttoainejäämistä muodostuneita hiukkasia.

Depositio- ja korroosiokokeet tehtiin itse suunnitellulla laboratoriomittakaavan depositio-korroosiolaitteistolla (DCA). Nimonic 80 A -materiaalin koekappaleissa havaittiin ”mustia saarekkeita” (15–33 p.-% S, loput pääosin Cr, Ni, ja Ti) käytettäessä SO2(g)-kaasua ja mallituhkahiukkasia (SAP) syöttönä. Näiden saarekkeiden koostumus viittasi niiden muodostavan ”sekasulfidin” ((Cr, Ti, Ni)Sx). Koska pohjakerroksessa hapen määrä oli hyvin alhainen, saarekkeet muodostuivat sisäisellä sulfidoinnilla. Samanlainen rikkipitoinen, ”mustista saarekkeista” muodostuva vyöhyke havaittiin kenttäkokeesta analysoidusta pakoventtiilistä. Kuitenkin termodynaamisten tasapainostabiilisuusdiagrammien perusteella nikkelikromaattien ja -sulfaattien (eli tyypin II kuumakorroosio) muodostumista ei täysin voi sulkea pois ilman lisätutkimuksia esim. XPS:n ja XRD:n avulla.

Academic dissertation

Supervising Professor(s):

Emeritus Prof. Simo Liukkonen/
Prof. Kyösti Kontturi
Helsinki University of Technology
Laboratory of Physical Chemistry and Electrochemistry

Supervisor:

Prof. Jorma Jokiniemi
VTT Fine Particles
University of Kuopio, Fine Particle and Aerosol Technology Laboratory

Preliminary examiners:

Prof. Jorma Keskinen
Tampere University of Technology
Department of Physics

Docent, Dr. Michael Spiegel
Department of Interface Chemistry and Surface Engineering
Max-Planck-Institute für Eisenforschung GmbH
Germany

Opponent:

Prof. Heinz Burtscher
University of Applied Sciences, Aargau
Institute for Aerosol and Sensor Technology
Switzerland

Helsinki University of Technology, Physical Chemistry and Electrochemistry

Preface

This thesis work was carried out at the Fine Particle team of VTT, previously known as the Aerosol Technology group of VTT Energy. I would like to thank my supervisor, Prof. Jokiniemi, and Prof. Kauppinen for their guidance and fruitful discussions when writing the papers. I am also indebted to my supervising Prof. Simo Liukkonen, for his continuous support and flexibility, especially during the completion of the doctoral studies. My pre-examiners, Prof. Jorma Keskinen and docent Michael Spiegel**,** are greatly acknowledged for their invaluable and constructive comments on the thesis. Dr. Pirita Mikkanen also deserves special compliments for really teaching me everything about how to carry out quantitative total particle mass and mass size distribution measurements with low-pressure impactors. I am also grateful to Dr. Jouni Pyykönen for constructive discussions and help on modelling. Dr. Jorma Joutsensaari, Mr Juha Kurkela, Dr. Tuomas Valmari, Dr. Ulrika Backman, Mr Ari Auvinen, and Mr Hannu Vesala are acknowledged for their invaluable help in carrying out the experimental measurements. I would also like to thank Prof. Kari Lehtinen for his help in designing the apparatus for the corrosion experiments, and Dr. Unto Tapper for carrying out the TEM analysis of the particles. Mr Raoul Järvinen also deserves special compliments for his invaluable help in building up all the experimental devices. I also like to thank all the members of our group for their encouraging attitude towards doctoral studies and for conducting excellent research.

I am also grateful for those who funded the work carried out in this thesis: Finnish Funding Agency for Technology and Innovation (Tekes), via the Flame II (Liekki II) and Materials for Energy Technology (KESTO) programmes, Wärtsilä, and VTT. Special compliments are due to the Emil Aaltonen Foundation, whose financial support made the finalising of the last two papers and writing the summary of this thesis possible.

Finally, many thanks to my wife Tiina for her support and encouragement, and for many discussions on how I should divide my time between my doctoral studies, writing this thesis, free time, and housework.

Contents

Appendices of this publication are not included in the PDF version.
Please order the printed version to get the complete publication
(http://www.vtt.fi/inf/pdf/)

List of original publications

A Lyyränen, J., Jokiniemi, J., Kauppinen, E. I. K., Backman, U., and Vesala, H. (2004) Comparison of different dilution methods for measuring diesel particle emissions. *Aerosol Sci. and Tech.* 38, 12–23.

B Lyyränen, J., Jokiniemi, J., Kauppinen, E. I. K., and Joutsensaari, J. (1999) Aerosol characterisation in medium-speed diesel engines operating with heavy fuel oils. *J. Aerosol Sci.* 30, 771–784.

C Lyyränen, J., Jokiniemi, J., and Kauppinen, E. I. K. (2002) The effect of Mg-based additives on aerosol characteristics in medium-speed diesel engines operating with residual fuel oils. *J. Aerosol Sci.* 33, 967–981.

D Jokiniemi, J. K., Pyykönen, J., Lyyränen, J., Mikkanen, P., and Kauppinen, E. (1996) Modelling ash deposition during the combustion of low-grade fuels. In: *Applications of advanced technology to ash-related problems in boilers* (Edited by Baxter, L. and DeSollar, R.). New York: Plenum Press. Pp. 591–615.

E Lyyränen, J., Jokiniemi, J., Kauppinen, E. I. K., and Silvonen, A. (2004) Corrosion studies with a new laboratory-scale system simulating large-scale diesel engines operating with residual fuels – Part II: Particle and deposit characteristics. *Fuel Proc. Technol.* 86, 329–352.

F Lyyränen, J., Jokiniemi, J., Kauppinen, E. I. K., and Silvonen, A. (2004) Corrosion studies with a new laboratory-scale system simulating large-scale diesel engines operating with residual fuels – Part I: Corrosion of Nimonic 80 A samples. *Fuel Proc. Technol.* 86, 353–373.

Author's contribution

This research started with preliminary aerosol modelling (ABC = Aerosol Behaviour in Combustion) calculations, completed in December 1994, to find out the main factors causing premature valve burning. On considering the model results, it was decided that more experimental data on the particles and their composition and morphology were needed in order successfully to clarify the mechanisms. This is how the experimental part of the exhaust ash particle characteristics research was started; it continued till early 1997. As there was growing interest in studying the deposition and corrosion caused by the exhaust ash particles deposited on the seat face surfaces of the exhaust valves in more detail, deposition and corrosion studies with new laboratory-scale equipment were started in mid-1997 and continued till early 2001.

The work presented in this thesis was carried out at the Aerosol Technology group of VTT under the supervision of Prof. Jokiniemi and Prof. Kauppinen. Paper A describes the effects of different dilution methods for measuring diesel particle emissions from an off-road four-stroke diesel engine. The effects were monitored by measuring the number size distributions with ELPI and DMA+CNC. The author of this thesis performed the experimental work and data analyses. Dr. Backman assisted in the DMA and TEOM measurements. The interpretation of the results was carried out in co-operation with Prof. Jokiniemi and Prof. Kauppinen.

Papers B and C describe exhaust ash aerosol characteristics in large-scale diesel engines operating with high ash content heavy fuel oils without and with a Mg-based additive. The author of this thesis performed the experimental work and data analyses. The interpretation of the results was carried out in co-operation with Prof. Jokiniemi and Prof. Kauppinen. Dr. Joutsensaari assisted in the sampling line design and carried out the DMA measurements.

Paper D describes the modelling results obtained from simulating ash particle deposition in large-scale diesel engine conditions. Dr. Pyykönen carried out the aerosol model calculations and wrote the paper. The chemical equilibrium calculations needed for adding chemical compound data into the aerosol model were performed by the author of this thesis.

Papers E and F describe deposition and corrosion phenomena on Nimonic 80 A samples in a new laboratory-scale system simulating large-scale diesel engines operating with residual fuels. A new system was designed to simulate the formation of the particles and their deposition on the studied sample slabs in such a way as it occurs in the real diesel engine environment. The author of this thesis performed the experimental work and data analyses. The interpretation of the results was carried out in co-operation with Prof. Jokiniemi and Prof. Kauppinen.

List of symbols and acronyms

Symbol	Name	Unit
λ	Relative air/fuel ($(A/F)_{rel}$) ratio	
ν	Kinematic viscosity	[mm^2/s]
ρ	Density	[kg/m^3]
$(A/F)_{rel}$	$(A/F)_{actual}/(A/F)_s$	
$(A/F)_{actual}$	True air/fuel ratio in the engine	
$(A/F)_s$	Air/fuel ratio for stoichiometric combustion	
CMD	Count median diameter	[nm]
DR	$Q_{tot}/(Q_{tot}-Q_d)$	
lpm	Litres per minute	[l/min]
N_{tot}	Total number concentration	[$\#/cm^3$]
ppm_w	Parts per million by mass	[mg/kg = µg/g]
Q_d	Dilution gas flow rate	[lpm]
Q_{tot}	Total flow rate after diluter	[lpm]
r_c	Compression ratio	
S_R	Saturation ratio	
T	Temperature	[°C]
w	Mass fraction	$0 \leq w \leq 1$

Acronym	Name
ABC	Aerosol behaviour in combustion
BLPI	Berner-type low-pressure impactor
CC	Catalytic cracking
CI	Compression ignition
CNC	Condensation nucleus counter
DCA	Deposition-corrosion apparatus
DI	Direct injection
DMA	Differential mobility analyser
DR	Dilution ratio
EDS	Energy dispersive spectrometry

ELPI	Electrical low-pressure impactor
ESP	Electrostatic precipitator
ESP-EM	Electrostatic precipitator for collecting electron microscopy samples
HA-HFO	High ash content heavy fuel oil
HC	Hydrocarbon(s)
HFO	Heavy fuel oil
ICP-AES	Inductively coupled atomic emission spectrometry
ICP-MS	Inductively coupled mass spectrometry
IDI	Indirect fuel injection
LFO	Light fuel oil
LFR	Laminar flow reactor
MDO	Marine diesel oil
PAH	Polyaromatic hydrocarbon(s)
PRD	Porous tube diluter
rpm	Rounds per minute
SAP	Synthetic ash particle(s)
SEM	Scanning electron microscope
SMPS	Scanning mobility particle sizer
TEM	Transmission electron microscope
TEOM	Tapered element oscillating microbalance
XPS	X-ray photoelectron spectroscopy
XRD	X-ray diffraction
XRF	X-ray fluorescence

1. Introduction

Various types of internal combustion engines are used for land and marine transport and power generation. Generally, the applications can be divided into three main classes according to the operating engine type: light-duty, heavy-duty, and large-scale engines. Light-duty engines are mainly used in automobiles and heavy-duty engines in buses and trucks. Large-scale, medium (750–1000 rpm)- or low speed engines have a different application range, covering marine applications, such as ships and tankers, and land-based power production. Light-duty engines can be operated using petrol or diesel, but heavy-duty and especially large-scale engines are exclusively fuelled by diesel and heavy fuel oil, respectively.

The fuel burned in the engines varies according to the application. Large-scale diesel engines are usually operated with heavy fuel oil (HFO). In the case of land-based power production engines the fuel can be of lower quality than HFO, meaning that the ash content of the fuel is higher (HA-HFO) or the fuel itself is of lower quality and contains heavier fractions. The reason for using these lower-grade fuels is purely economic. To be able to compete successfully in power production with gas turbines, which have greater thermal efficiency and use cleaner fuel, the thermal efficiency of large-scale diesels has to be increased and/or the fuel costs have to be reduced. However, operation with low-grade fuel oils may lead to severe hot corrosion and erosion problems. Hot corrosion usually refers to sulphidation-accelerated oxidation phenomena at high temperatures (approx. $T \geq 500°C$), coupled with deposits of molten salts (Kofstad, 1988).

A first step in understanding the mechanisms of hot corrosion and erosion is to identify the particle formation mechanisms. In large-scale diesel engines these mechanisms are, generally, different from those in light-duty or heavy-duty engines. This is the consequence of different engine specifications and fuel. The fuel in large-scale diesel engines usually contains a high fraction of aromatics and ash (approx. 0.1 wt. %), which is composed of vanadium, sodium, calcium, nickel, magnesium, aluminium, and silicon. In addition, the sulphur content of the fuel oil is usually high, approx. 3 wt. %. Therefore, low-melting vanadylvanadates may form (Kerby and Wilson, 1973). The high calcium content of the lubricating oil may also have a profound effect on the corrosion of some materials/coatings (Umland and Ritzkopf, 1975).

The number and mass size distributions from diesel engines can provide valuable information on particle formation. There are numerous articles, reviews, and books on the formation and structure of particles in diesel engines (Baumgard and Johnson, 1996; Dolan et al., 1975; Kerminen et al., 1997; Amann and Siegla, 1982; Burtscher, 1992; Heywood, 1989). All of these references, however, deal mainly with either light-/heavy-duty applications and/or soot formation in diesel engines operating with non-residual fuel oils with a low sulphur content and only traces of, or no, metal impurities. This, together with different engine configurations, can severely affect particle formation in comparison to large-scale engines. Therefore, the approach followed in these articles is not directly applicable to the problem encountered here. Only recently have publications become available that deal with particle formation in large-scale diesel engines (Kasper et al., 2001; Lyyränen et al., 1999 (Paper B); Lyyränen et al, 2002 (Paper C); Rodriguez-Maroto et al., 2001).

To obtain representative particle samples from diesel engines usually requires dilution of the sample flow. The optimum dilution system for the purposes of the experimental set-up depends greatly on the focus of the measurement. The aim may be to simulate the dilution effect when the exhaust gas enters the atmosphere and dilutes, i.e. to simulate atmospheric dilution. The target may be to preserve the number size distributions in as unbiased a manner as possible from the measurement and dilution set-up artefacts and to produce a so-called "real" distribution of the exhaust gas as it would be observed inside the exhaust pipe. This may be particularly important if the link between atmospheric dilution and the undiluted exhaust gas needs to be established. Regardless of the dilution system used, the methods are still the same: to control the dilution ratio (DR), dilution rate, temperature, and residence time to prevent the nucleation of hydrocarbon (HC) species and, in the case of high S-content fuel oils, the nucleation/condensation of sulphuric acid. Nucleation is a competing process with adsorption and condensation on pre-existing soot particles. Thus the dynamic behaviour of this vapour-particle system in the dilution process will determine the number size distribution after dilution and cooling.

Particle and deposit characteristics play an important role in studying corrosion and erosion phenomena in combustion systems. Furthermore, the corrosion and erosion of different materials nearly always involve a growing deposit layer. To determine the effects and mechanisms of corrosion and erosion, the morphology,

structure, and composition of the depositing particles and the deposit are important. Additionally, the chemical reactions taking place in the deposit layer need to be recognised in order to find out how the depositing particles start to react/transform into the actual deposit. The formation of the deposit may have crucial effects on the corrosion/erosion mechanisms; these mechanisms can be different if the deposit is absent from the surfaces under corrosive/erosive attack.

There are many studies and reviews on coal, biomass, and black liquor deposits in different boilers (Baxter et al., 1998; Bryers, 1996; Srinivastava and Godiwalla, 1997). However, the gas atmosphere and conditions in the boilers, even when operating with heavy fuel (HFO) or residual fuel oils, are not relevant to those prevailing in large-scale diesel engines, because the relative air/fuel ratio, $\lambda=(A/F)_{rel}$, is much higher, approx. twice as high, in the diesel engine. In addition, the depositing and corrosive/erosive elements are different, consisting mainly of chlorine (Cl), sulphur dioxide ($SO_2(g)$), and alkalis in boiler conditions. In large-scale diesel engines or oil-fired boilers, however, there is significantly less Cl, except in marine applications, where the harmful Cl originates from the cooling water and intake air. On the other hand, the quantity of vanadium (V) and sulphur (S) may be very high, depending on the quality of the fuel oil. In particular, Venezuelan crude oils are notorious for containing a lot of V and S. Other detrimental elements present in the fuel oils are mainly Ni, Na, and Ca, though in diesel engines the main source of Ca is the lubricating oil used.

When studying corrosion in more detail with several different materials and gas atmospheres, the experiments are usually performed on a laboratory-scale. There are many articles concerning the corrosion phenomena of different valve materials in a simulated diesel environment. These experiments, however, mainly consider studies performed in an autoclave with a suitable atmosphere and applying synthetic ash to the samples at regular intervals (e.g. 50 h) (Nicholls and Stephenson, 1990; Nicholls and Triner, 1990; Nicholls, 1993; Kofstad, 1988). Corrosion studies have also been performed in burner rigs (Seiersten et al., 1987). These laboratory results are usually verified by field tests. Although the corrosive deposit, i.e. ash, has the correct chemical formula, the formation of the corrosive ash layer as the particles deposit on to the samples is not taken into account. Additionally, the possible transformation of the deposited particles when they start to react to form a corrosive ash deposit is not dealt with.

1.1 Objectives of the study

The objectives of this study can be divided into three main sections:

1. Comparison of different dilution methods for measuring large-scale diesel engine exhaust gas particles;
2. Characterisation of exhaust gas particles in large-scale diesel engines operating with low-grade residual fuel oils and how a Mg-based fuel oil additive affects the exhaust gas particles;
3. Studying deposition and corrosion on sample slabs exposed to simulated large-scale diesel fuel ash particles and gas flow in a laboratory-scale system and to verify that the results correspond to those obtained from full-scale engine tests.

The focus of the dilution methods section of this work was to compare the results obtained with different dilution systems. The target was to achieve an unbiased real number size distribution from a diesel engine, excluding the simulation of atmospheric dilution when the exhaust gases leave the exhaust pipe. Since total particle number concentration and number size distribution are very sensitive to changes in measurement conditions, they were selected as parameters to compare number concentrations and size distributions in different dilution systems.

In the particle characterisation section the objective was to study the formation of particles and their morphology and chemical composition in large-scale diesel engines operating with low-grade residual fuel oils. Furthermore, the effect of a Mg-based fuel oil additive on the exhaust gas particles was investigated. The main function of the additive was to reduce/hinder the formation of corrosive deposits, especially on the seat face of the exhaust valves. Prior to the experimental work, modelling of the diesel combustion was carried out in order to identify the possible chemical compounds present in the system (Jokiniemi et al., 1996). It was found that nickel oxide formed the first particles by nucleation. The focus of this study was not on soot formation, although some aspects are discussed. The results presented illustrate fine ash formation and elemental composition in diesel engines operating with residual fuel oils, with or without a fuel oil additive.

The target in the deposition and corrosion section was to study the deposition formed at the surfaces of the Nimonic 80 A samples and their corrosion when exposed to simulated large-scale diesel fuel ash particles and gas flow in a laboratory-scale system. To accomplish this, a new deposition-corrosion apparatus (DCA) was designed. With this set-up the formation of the exhaust ash particles, gas composition, and deposition and corrosion on to the samples occurs in a similar way as in large-scale engines. The system simulates the conditions in the diesel engine, except for the high pressure during work stroke and the cyclical mechanical contact between the cylinder head and valve seat face. Furthermore, the morphology and chemical composition of synthetic diesel ash particles was also investigated in order to find a possible relationship in how the characteristics of the particles change when they are deposited on to the samples.

2. Literature review

2.1 Large-scale diesel engine fuels and combustion characteristics

There are many different fuel oils that can be burned in large-scale diesel engines: heavy fuel oils (HFO), marine diesel oils (MDO), gas oils, oil-in-water emulsions, Orimulsion, which is a bitumen-in-water emulsion (Miller and Srivastava, 2000), etc. According to Concave (1998), HFO is a general term, and many other names exist to describe this product range: residual fuel oil, bunker fuel, bunker C, fuel no. 6, industrial fuel oil, marine fuel oil, and black oil. Generally, the prefixes heavy, medium, or light, when applied to a fuel oil, indicate the viscosity and density of the product.

Chemically, HFOs resemble asphalt, and therefore they are considered to be stabilised suspensions of asphaltenes in an oily medium. Residual oils also contain organo-metallic compounds derived from the original crude oils, the most important trace being vanadium (V). For example, Caribbean (Venezuela) and Mexican crude oils contain high amounts of V, which leads to high V-content HFOs. Other important metallic elements present in HFOs are Ni, Fe, K, Na, Al, and Si. Al and Si in particular originate from the catalyst fines in the CC unit at the refinery. Typical HFO properties are presented in Table 1.

The critical parameters concerning the combustion properties of HFOs are, generally: carbon and aromatic content, heating value, and ash content, which also includes the metallic constituents of the fuel, i.e. V, Na, Ni etc. typically present in heavy fuel oils.

In internal combustion engines, the critical parameters are: how the fuel and oxidant are transported into the reaction chamber(s), i.e. the cylinder(s), how the oxidant supply is arranged, how the fuel-air mixture is ignited, and what the characteristics of the resulting exothermic gas-phase reaction, i.e. the flame, are (Heywood, 1989). In this study the engines are four-stroke, large-scale diesel engines for power plant and marine applications. Combustion in these engines can be characterised by three terms; turbo-charging, direct-injection (DI), and compression-ignition (CI), i.e. diesel engines (Fig. 1, Paper B).

Table 1. Typical properties of heavy fuel oils (w = mass fraction, $0 \leq w \leq 1$), adapted from Concave (1998).

Property	Typical range
ν [mm^2/s], T = 100°C	6.0–55.0
ρ [kg/m^3], T = 15°C	950–1010
w(carbon residue)	< 0.22
w(ash)	< 0.002
w(water)	< 0.01
w(sulphur)	Inland: < 0.035 Marine: < 0.05
Vanadium [mg/kg = ppm_w]	< 600
Aluminium + silicon [mg/kg]	< 80

Typical mechanical efficiencies of large-scale turbo-charged DI diesel engines range from 43 to 50%, depending on the engine size and operational conditions (cylinder bore and pressure during the compression stroke). Compression ratios (r_c) for these engines are in the range of 12–24 (Silvonen, 1996). The peak pressures and temperatures are also very high. The maximum temperature is approx. 2200–2500°C at the beginning of the expansion (work) stroke and the maximum pressure approx. 160–180 bar during the compression stroke.

2.2 Effects of dilution system on diesel particle emissions

There have been many studies on the formation, characteristics, and transitions of diesel exhaust gas particles related to the measuring set-up and dilution techniques, especially with the industry standard dilution tunnel (Dolan et al.,

1975; Abdul-Khalek et al., 1998; Kittelson, 1998; Shi et al., 1999; Shi and Harrison, 1999; Shi et al., 2000). As the purpose of the dilution tunnel is to simulate the atmospheric dilution process as the exhaust gases enter the atmosphere, there has been criticism of how well the tunnel actually succeeds in this (Kittelson, 1999; Maricq et al., 2001). The study by Maricq et al. (2000) also compares the results obtained by ELPI and DMA+CNC and deals with the possible problems in this comparison. Kittelson and Johnson (1991) also extensively studied the possible causes of variations in number size distributions measured with dilution tunnel set-ups. There is also a recent and comprehensive review article by Burtscher (2005) on particle characterisation from light- and heavy-duty diesel engines. This review article focuses specifically on dilution techniques and systems for measuring the particles.

2.3 Large-scale diesel engine particle emissions

Soot formation is an essential part of the particle emissions of diesel engines. It has been studied widely, and several articles and reviews describe the formation, morphology, and composition of soot (e.g. Amann and Siegla, 1982; Burtscher, 1992; Ishiguro et al., 1997; Burtscher et al., 1998). PAH emissions should also be considered when the health effects of exhaust particles are being studied. Rodriguez-Maroto et al. (2001), Cooper (2001), Cooper et al. (1996), and Bonk and Lange (1994) studied PAH emissions from medium-speed diesel engines operating with different fuel oils. In this study, however, the focus is neither on soot formation nor on PAH emissions. Therefore, the formation, morphology, and composition of soot particles are not treated in detail in the literature review.

Large-scale diesel engines operate with very high relative air-to-fuel ratios ($(A/F)_{rel} = \lambda \approx 2$ and higher) at full load, which should ensure almost complete combustion without soot formation. However, in diesel combustion local atmospheres in the cylinder can vary greatly, from highly oxidising to highly reducing. Therefore, the mixing of the charge air and injected fuel plays a critical role in the formation of (soot) particles.

There have been extensive studies on the total number and mass concentrations and number and mass size distributions in diesel engines by e.g. Kasper et al. (2001), Rodriguez-Maroto et al. (2001), Cooper (2000) and Brehob et al. (1983).

Generally, all the studies indicated that the mass concentrations were increased when operating with lower-quality residual fuel oils (high ash content, > 0.1 wt. %), compared to heavy fuel oils. Another important parameter was engine load. However, engine load did not have a very significant effect on the bimodal particle size distributions, which typically had modes at 70–100 nm and 7–10 µm and at 40–70 nm in mass and number size distributions, respectively.

Diesel ash particle morphology and composition have been studied by e.g. Paro (2001), Kasper et al. (2001), and Brehob et al. (1983). Generally, residual fuel oil ashes contained more inorganic elements than heavy fuel oils. In medium-speed diesel engines exhaust gas particles contained (in wt. %) 25 of soot, 10 of hydrocarbons (HC, originating from the fuel and lubricating oil), and 65 of ash (metal oxides, sulphates; Paro, 2001).

2.3.1 Effects of fuel and fuel additives

Bonk and Lange (1994) found that if the sulphur content of the fuel oil (1.5–3 wt. %) were increased and the relative air-to-fuel ratio ($(A/F)_{rel} = \lambda = 1–2.5$) were decreased simultaneously, the particle mass concentrations increased significantly (52–170 mg/m^{3}n). If only the sulphur content of the fuel oil were increased the increase in particle mass concentrations was clearly less than in the previous case. According to the authors, this was the consequence of the increased amount of sulphate in the particles. In addition, increasing the aromatic (37.5–50 wt. %) and sulphur content (0–2.8 wt. %) of the fuel oil increased the particle mass concentrations significantly (30–210 mg/m^{3}n). If the fuel oil has a high aromatic content this causes ignition delay and, therefore, higher particle mass concentration.

Adding water to fuel oils, i.e. emulsifying, gave results that depended on the quality of the fuel oil; the addition of small amounts of water increased the particle mass concentrations for fuel oils with a high aromatic content (46 wt. %) and decreased them for fuel oils with a lower aromatic content. For gas oil the effect of water addition was almost insignificant. Similar results were found by Brehob et al. (1983); increasing the amount of water added increased the particle mass emissions.

Heavy fuel oil additives are usually Mg-based compounds (Bryers, 1996; Cortes et al., 1990; Scott, 1977; Kukin, 1973). However, their primary target has mainly been to prevent the formation of highly corrosive vanadylvanadate compounds that contain mainly vanadium, sulphur, and sodium of different compositions and have low melting points (Bryers, 1996; Kerby and Wilson, 1973). Miller and Srivastava (2000), Reynolds and Pachaly (1999), Lin and Sheu (1997), Cortes et al. (1990), Kukin (1973) all found similar effects with Mg-based additives in HFO-fired oil boilers; the particle mass concentrations decreased clearly and SO_3(g) concentrations increased. The main mechanisms for reduced particle emissions were: easily ionisable elements that reduce soot formation; elements that enhance OH-radical formation and increase soot oxidation, and elements that get absorbed by soot and increase their combustion rate (Reynolds and Pachaly, 1999). Similar mechanisms are also reported in more detail by Howard and Kausch (1980). However, no results on the effects of Mg-based additives on emissions and particles from large-scale diesel engines have been published. Because the fuel oil is similar to that used in oil boilers, it is to be expected that a Mg-based additive might have similar effects in engines, even though the combustion process is different.

Other types of additives have also been intensively studied. Seeding a direct injection (DI) diesel engine type flame with e.g. ferrocene ($Fe(C_5H_5)_2$; Mitchell, 1991; Zhang and Megaridis, 1996; Kasper et al., 1999) can enhance soot oxidation, thus reducing emissions. Cerium has also been studied as a fuel oil additive (Burtscher et al., 1999; Skillas et al., 2000). It has been proposed that a Ce additive mainly reduces the concentration of organic carbon (OC), but not so much the concentration of elemental (EC) or black carbon (BC) in the exhaust particles.

2.4 Deposition and corrosion of exhaust valves in large-scale diesel engines

Deposition and corrosion phenomena on the exhaust valves of large-scale diesel engines depend on many different parameters, such as actual valve design, material selection, and the fuel and lubricating oil and fuel oil additives used. As the focus of this study is more on existing valve materials and the deposition and corrosion phenomena associated with them, the effect of valve design and different materials on deposition and corrosion is not treated.

2.4.1 Effects of lubricating oil and fuel oil additives

The effect of lubricating oils on valve corrosion can be remarkable. The amount of Ca present in lubricating oil varies greatly, depending on the quality and manufacturer of the oil. Additionally, other oil additives which are used to improve the properties of the lubricating oil, such as Zn, P, Ba, and Pb, can have detrimental effects on engine components. However, the detrimental impact of Ca on exhaust valves depends greatly on the valve material. Umland and Ritzkopf (1975) found that Ni-based alloys were less sensitive to high Ca contents than Co-based alloys. However, the test matrix was limited to two materials and hard facings. In addition, residual fuel oils may contain various levels of catalytic fines consisting mainly of alumina and silicates used as catalyst carriers in refinery processes. These fines can cause wear in cylinder liners, injectors, valve faces etc. (Fairbanks et al., 1984).

The fuel oil additives used in burning heavy fuel oils are usually Mg-based compounds (Bryers, 1996; Cortes et al., 1990; Scott, 1977; Kukin, 1973). The advantage of using these additives is that magnesium reacts with vanadium to form magnesium vanadylvanadates that have melting points that are clearly higher than those of their sodium counterparts. Thus the deposits are no longer molten/highly sintered and the detrimental fluxing of the elements is hindered. Moreover, the structure of the deposit is transformed into a more porous and less adhesive form (Bryers, 1996; Kerby and Wilson, 1973).

To attain these favourable effects, the magnesium-vanadium weight ratio should be approx. 1.5:1 (3:1 in molar ratio [Kukin, 1973]). Even higher Mg-V weight ratios are beneficial and silicon can also be advantageous (Scott, 1977). However, especially in oil-fired furnaces, the use of Mg-based additives causes other problems. The deposits can build bridges between heat exchanger tubes because of increased ash loading and thus hinder effective heat transfer (Kukin, 1973). Increased ash loadings may also cause problems.

2.4.2 Deposition and corrosion studies

Deposition, corrosion, and erosion mechanisms in diesel engines are the sum of engine design, material selection, fuel, and lubricating oil. The corrosion itself

causes damage to the materials and components used in diesel engines and gas turbines, but it cannot be the sole cause of material and engine failures. The interaction of corrosion and erosion causes the severe damage found in engine and turbine systems operating on residual fuel oils (Fairbanks et al., 1984).

Generally, when several different materials and gas atmospheres need to be studied, the experiments are performed on a laboratory-scale in order to cut costs. Seiersten et al. (1987) studied corrosion and also some deposition structure formed on rotating (600 rpm) cylindrical rods in a high-velocity burner rig with a 200–300-m/s gas velocity. They suggested a mechanism whereby the preformed oxidation layer starts to dissolve in the molten deposit, followed by a precipitation of vanadates or oxides near the outer surface of the deposit. Nicholls and Stephenson (1990) and Nicholls (1993) studied different valve materials in simulated diesel environments, e.g. in an autoclave with a suitable atmosphere and applying synthetic ash at regular intervals (e.g. 50 h) on to the samples. The actual deposit formed in these tests was not studied, but the scales building up on the surface of the base materials were identified with SEM/EDS as being mainly V, Cr, and Ni or V, Cr, and Fe containing mixed oxides. They concluded that the most important factor affecting vanadic corrosion may be the contaminant flux rate (CFR). On the other hand, with full-scale engine tests (test times 100–300 h) with a residual fuel oil containing 331 ppm V, 35 ppm Na, and 3.65 wt. % S, Nicholls (1994) found that corrosion rates were about 30 times greater in the field tests. According to the author this was mainly caused by the higher contaminant flux rates present in the full-scale engines.

Although there are many studies of hot corrosion mechanisms at high temperatures, they have mainly concentrated on sodium sulphate-induced hot corrosion on different metals/alloys and presume that a molten phase is formed on top of the protecting metal oxide. This molten phase further enhances the corrosion by acidic or basic fluxing (Goebel et al., 1973; Luthra and Shores, 1980; Rapp, 1987; Rapp and Zhang, 1994). Kofstad (1988), Rapp (2002), and Rapp and Zhang (1994) report that the key issue in the fluxing mechanism at the interface between the deposit and the metal scale is the formation of a molten deposit layer that provides the fluxing matrix. The fluxing matrix is not usually very thick.

The hot corrosion mechanisms concerning the simultaneous effect of sodium and vanadium compounds in diesel engines, i.e. high oxygen and sulphur dioxide content, are not so well understood. Iyer et al. (1987) studied the hot corrosion cracking of Nimonic 80 A material with kerosene doped with sulphur (2.5 and 5 wt. %), sodium, or vanadium (both 10–40 ppm). They concluded that at 600°C the sulphur from the fuel oil reacts with the chromium to form chromium sulphide, depleting the alloy of chromium. As the mechanism is not self-sustaining, the attack is not severe. However, at higher temperatures (700°C) a eutectic melt is formed and the sulphur cannot escape into the atmosphere as in the previous case. The mechanism thus becomes self-sustaining.

On the other hand, Jones (1988) states that V_2O_5 has been reported as diminishing the Na_2SO_4 hot corrosion of nickel by forming $Ni_3(VO_4)_2$. Increasing the sulphur level of the fuel oil can increase the V_2O_5 activity in the salt deposit. Moreover, he suggests that the propagation of the corrosion at the metal interface does not necessarily involve a liquid phase (sulphates or sulphides) but advances by solid/gas transport, enhanced by the trace vanadium in the oxide lattices. As the lowest oxidation state of V is normally +2, no equivalent of a liquid sulphide occurs in vanadic hot corrosion.

3. Methods

3.1 Engines, fuel, lubricating oil, and materials

The engine types studied varied from a small auxiliary marine diesel engine to a large power plant-type engine. All engines were four-stroke, medium-speed (750–1000 rpm at 100% load), direct injection (DI) diesel engines with four valves per cylinder and equipped with turbocharger(s) (Fig. 1, Paper B). The normalised displacement of the engines was 0.07 for small engine 1, 0.1 for small engine 2, and 1 for the large engine. The normalised displacement is the total displacement of the diesel engine in relation to the large engine, i.e. the total displacement of this engine is set to unity. The exhaust gas temperatures of the engines after the turbocharger varied from 300 to 400°C, depending on the engine size and load (Papers B and C).

The fuel oil was either heavy fuel oil (HFO) or high ash content heavy fuel oil (HA-HFO, ash content 0.1 wt. % or higher). The main constituents of the ash were vanadium (V, 400 ppm_w), sodium (Na, 50–60 ppm_w), and nickel (Ni, 50 ppm_w). The sulphur content (S) was also high, being approx. 2.5 wt. %.

The main components of the lubricating oil used in these engines were calcium, zinc, phosphorus, and magnesium. The Ca content of this lubricating oil was high, being approx. 1 wt. %.

In the deposition-corrosion experiments (duration 6 days [144 h]), the material sample studied was Nimonic 80 A (Cr 20, Fe 3.0, Ti 2.4, Al 1.4, Si 1.0, C 0.1 wt. % and Ni as balance). The gas atmosphere (SO_2(g), O_2(g), and N_2(g)) and the composition of the reagent solution for producing synthetic ash particles (SAP) were selected so that they corresponded to the gas atmosphere in the engine and the composition of HA-HFO. The reagents were dissolved in a 7 wt. % HNO_3 solution containing vanadium pentoxide (V_2O_5), nickel nitrate ($Ni(NO_3)_2 \cdot 6H_2O$), and sodium nitrate ($NaNO_3$) or de-ionised water as a solvent, and the other reagents were the same, except that the vanadium species was $VOSO_4 \cdot 3H_2O$ (Papers E and F). The sample temperatures ranged from 700 to 750°C.

Two different reagent solutions were prepared to study the effect of SO_2(g) on the particle and deposit formation and corrosion. Therefore, the water-soluble $VOSO_4 \cdot 3H_2O$ had to be replaced with vanadium pentoxide for one experiment (1/00, Paper F), as no nitrate compound was available. Because vanadium pentoxide is not water-soluble it was dissolved in a 7 wt. % HNO_3 solution. Water-soluble, nitrate-based reagents were preferred for easy dissolution.

3.2 Experimental methods

Exhaust gas particle samples from the large-scale diesel engines were characterised with a number of methods and equipment based on aerosol technology. These techniques provided the basis for determining particle formation mechanisms based on the measured total number and mass concentrations and number and mass size distributions. Supplementing these methods with a group of analytical tools, the total particle elemental mass concentrations and mass size distributions, together with individual particle morphology and chemical composition, were obtained. Combining and interpreting the data from these sources made it possible to clarify the history of the exhaust gas particles.

For the deposition-corrosion studies a new facility was designed. The deposition-corrosion system consisted of an aerosol (synthetic ash particle, SAP) and gas feeding system, a heated inlet, a three-zone laminar flow reactor (LFR) furnace, and a deposition-corrosion apparatus (DCA). The aim of this system was to simulate the formation of the particles and their deposition on the samples studied in the same way as it occurs in full-scale diesel engines as the exhaust valve opens.

3.2.1 Sampling and measurement methods

In the following section a short description of the experimental techniques and equipment used in this study is provided. For more thorough information the required references are provided.

A *porous tube diluter (PRD, dilution probe)* was used to dilute the exhaust gas particle samples from the engines (Papers A–C) and the synthetic ash particle (SAP) samples generated in the deposition-corrosion experiments (Paper E).

PRD is a coaxial cylindrical diluter in which the dilution air flows through a porous tube (pore size 20 µm) into the inner tube, thus sheeting the aerosol flow from deposition and thermophoresis (Auvinen et al., 2000). In addition, the dilution air and the diluter were heated to the exhaust gas temperature at the measurement location to avoid sulphuric acid condensation and "unwanted" nucleation during dilution. The need for the dilution air and diluter heating in these conditions was also found necessary based on the results presented in Paper A. Heating is also the easiest way to dilute the sample flow without major sulphuric acid condensation and "unwanted" nucleation.

An *ejector-type diluter (ED)* was used to dilute the sample flow prior to the entrance to the DMA (Papers A–C). The diluter consists of an inlet nozzle, an annular nozzle, and a mixing chamber. Cleaned dilution air flows through the annular nozzle, which sheets the flow at the aerosol inlet nozzle. Because of the under-pressure developed, the aerosol flow is drawn inside the diluter and mixed with the dilution air in the mixing chamber. If the absolute pressure at the inlet nozzle is the same as in the mixing chamber, the dilution ratio is independent of the dilution airflow rate (Koch et al., 1988).

A *Berner-type low-pressure Impactor (BLPI)* was used to measure the mass size distribution of the particles in the exhaust gases after the engine turbocharger (Papers B and C) and in determining the synthetic ash particle (SAP) mass size distributions (Paper E). The BLPI has a total of 11 collection stages, where the aerosol is directed through orifices lying against a flat collection plate. The uppermost stage (11) collects particles whose aerodynamic diameter is larger than 10 µm and the lowest stage (1) particles whose aerodynamic diameter is 0.01–0.02 µm. When passing through several successive impactor stages the aerosol is classified into several different size classes (Berner and Lürzer, 1980; Berner et al., 1979; Hillamo and Kauppinen, 1991; Kauppinen, 1992).

A *differential mobility analyser (DMA)* was used to measure the number size distribution of the particles after the engine turbocharger (Papers A and B). Prior to entering the DMA the large particles (> 0.7 µm) are removed by a pre-impactor mounted on the DMA inlet. In the DMA the aerosol sample is separated according to the electrical mobility of the particles so that only a selected size class is allowed to pass through (Knutson and Whitby, 1975).

A *condensation nucleus counter (CNC)* was used to measure the size classified particle number concentration from DMA (Papers A and B). In the CNC supersaturated vapour (in this case butanol) is condensed on the aerosol particles and makes the particles grow into larger, more easily detectable droplets. In the cooled condenser tube these particles will pass through an optical detection system, which counts the individual pulses caused by each particle for low sample concentrations. If the sample concentration is high, the light scattered by all the particles in the sensing zone is measured and compared with calibration levels, and the concentration can thus be obtained (Cheng, 1993).

A *point-to-plane electrostatic precipitator for electron microscopy samples (ESP-EM)* was used to sample individual particle samples from the exhaust gas streams of the engines (Papers A–C) and in the deposition-corrosion experiments for SAP particles (Paper E; Yeh, 1993). The deposition efficiency of the point-to-plane ESP was studied by Laskin and Cowin (2002). They found that the net deposition efficiency was not better than 50% for their device (point-to-plate distance 3 mm, 5kV voltage, and 0.3 lpm flow through the ESP) for particles in the size range of 0.1–2.0 μm. The samples were collected on Holey carbon-coated copper grids.

Deposition-corrosion apparatus (DCA). To simulate the flow past the exhaust valve during the exhaust stroke of a large-scale diesel engine as well as possible, a DCA with a jet plate just in front of the tested sample slab holders was designed (Papers E–F). The jet plate contains altogether 60 orifices (0.5 mm in diameter), with four columns and three rows in each of five groups of orifices. The size of the orifices was designed so that the collection efficiency is at its maximum for particles about 1–2 μm in size. Four sample slab holders were mounted behind the jet plate. Because of the orifices in the jet plate there is a pressure difference over the plate that causes the flow to accelerate through the orifices to a speed of about 100 m/s. This is about the same magnitude as that observed in large-scale diesel engines.

Tapered element oscillating microbalance (TEOM). A 1400a-type TEOM (Patashnick and Rupprecht, 1986; Patashnick and Rupprecht, 1991) was used to monitor the mass concentration during the synthetic ash particle feed (Papers E and F). The particles were collected on a filter, which was placed on top of a transversely vibrating hollow rod. The sample flow was drawn through the filter

and the rod with a pump. Because the rod oscillates as a harmonic oscillator the mass of the oscillating element (the hollow rod and the filter) can be calculated from the vibration frequency of the rod.

3.2.2 Analytical techniques

ICP techniques were used to analyse the bulk elemental mass concentrations of the BLPI samples. Both inductively coupled plasma mass spectroscopy (ICP-MS) and atomic emission spectroscopy (ICP-AES) were utilised. Prior to the analyses with ICP-MS and ICP-AES, the samples were dissolved either in an $HF\text{-}HNO_3$ mixture at room temperature or in 7 mol/dm^3 HNO_3 at 90°C, respectively. Metcalfe (1991) provides more information on the analysis techniques with ICP-AES and Tanner et al. (2002) on ICP-MS.

Individual particle samples were analysed with a Leo DSM 982 Gemini field emission (FE) SEM with a Pioneer Norvar Si(Li) EDS detector with Noran Voyager Type 4 software and a Jeol 2010 200 kV TEM with a PGT EDS analyser. For further information on the SEM, Joy (1992) and Goldstein et al. (1992), on the TEM, Buseck et al. (1992), and on the EDS, Goldstein et al. (1992), Lifshin (1994), and Hall (1992) provide a thorough approach.

4. Results and discussion

4.1 Particle characteristics in medium-speed diesel engines

4.1.1 Number concentrations and size distributions

Number concentrations for particles smaller than 0.7 μm were measured after the engine turbocharger (Fig. 1, Paper B). The number concentrations were normalised (relative concentrations) with the large engine at a 50% load with HA-HFO (base case, $c_{tot} \equiv 1$). The highest number concentrations were observed in small engine 1 (relative engine size 0.07) at a 110% load and high ash content heavy fuel oil (HA-HFO), about threefold compared to the base case. The total number concentration was lowest in small engine 1 at a 100% load and HFO, about 30% of the base case. The difference in number concentrations between the two small engines marked as 1 was mainly caused by the different fuel oil composition. The ash content of the HA-HFO is about six times that of the regular HFO. Increasing the load of the large engine (relative engine size 1) from 50% to 110% doubled the total number concentration. The lower total number concentrations at partial loads can partly be explained by the larger amount of oxygen (higher relative A/F ratio) present in the combustion chamber; with a 50% load, $\lambda = 2.9$ and with a 110% load, $\lambda = 2.4$ (Table 1, Paper B). This may also be interpreted that feeding less fuel oil to the same gas volume produces less particles and soot. The lower pressure in the cylinder can also affect the number concentrations.

The exhaust ash aerosol number size distribution for small engine 1 (relative engine size 0.07) had a mode at about 55 nm. Varying the engine load from 90–110% using HFO or HA-HFO did not seem to have any remarkable effect on the number size distribution mode. For the large engine (relative size 1) the number size mode was at about 40–45 nm, regardless of the load (Fig. 3, Paper B). The number size mode was in slightly smaller particles in the large engines than in the small ones. This can be caused by better air and fuel mixing and longer residence times in the large engines, leading to a more complete combustion of the fuel oil and thus a decrease in the amount of particles formed.

4.1.2 Mass concentrations and size distributions

The mass concentrations were normalised in the same way as the total number concentrations (large engine at 50% load and HA-HFO fuel oil, base case; Paper B). The total mass concentration was lowest for the large engine with HA-HFO fuel oil at 110% load, about 70% of the base case. The highest mass concentrations, as number concentrations, were observed with small engine 1 (relative size 0.07) at 110% load and HA-HFO fuel, over twice as many compared to the base case. The mass concentrations for small engine 2 (relative size 0.1) at 100% load and HA-HFO were about 60% higher than in the base case. The mass concentration for small engine 1 with HFO fuel oil was about the same as the base case (large engine at 50% load and HA-HFO) mass concentration.

The mass size distributions in the size range 0.01–15 μm (aerodynamic diameter) were bimodal. These distributions were normalised in the same way as described earlier. The small particle mode was at under 0.1 μm and the large particle mode at about 10 μm (Fig. 4, Paper B). However, particles throughout the measured size range were present. For small engine 1 with HFO and a 100% load, the mass size of the small particle mode was at about 0.08 μm and the large particle mode at 10 μm. With HA-HFO and a 110% load, the small particle mode shifted to about 0.1 μm. The mode for small engine 2 with a 100% load was also at 0.1 μm. For the large engine with either a 50% or 110% load the mass size small particle mode was at about 0.06 μm, but there was no mode at 10 μm at 110% load.

The mode at 10 μm in the mass size distributions was not observed in all of the studied process conditions. The particles in this mode may result from incomplete combustion of the fuel oil droplets or be produced by the re-entrained particles from the surfaces of the combustion system (turbine blades, exhaust pipe surfaces, etc.). Re-entrained particles would also explain the more or less random occurrence of the 10-μm mode. Re-entrainment of the particles from the combustion chamber walls of a diesel engine was studied by Abu-Qudais and Kittelson (1997). They concluded that soot concentrations can be about 45% higher during blowdown than in the displacement phase. This was mainly caused by the high velocities and highly shearing flow during blowdown.

4.1.3 Individual diesel ash particle morphology

Studying HA-HFO fuel oil ash particle surface morphology revealed two main classes of particles, fine mode ones, 40–100 nm in diameter, and coarse mode ones, about a few microns in size, although the sizes may vary.

The fine mode (40–100-nm) particles are referred to as nucleated particles. Nucleation is defined as the formation of new particles from a supersaturated vapour without the assistance of condensation nuclei or ions. This requires the saturation ratio (S_R) of that vapour to be over 1. It is defined as the partial pressure of the vapour (p) divided by its saturation vapour pressure (Hinds, 1999):

$$S_{R,i} = \frac{p_i}{p_{s,i}} \tag{1}$$

The coarse mode (> 0.4-µm) particles are referred to as re-entrained particles, as their occurrence in the mass size distributions is more or less random. Other important distinguishable particle classes contributing to the coarse mode consisted of the particles formed from the fuel oil droplet residue and the particles indicating mechanical abrasion (sharp-edged particles).

The fine mode particles, 40–100 nm in diameter, were almost spherical (Fig. 5a, Paper B) and were generated by the nucleation of the volatilised fuel oil ash species (mainly V, Ni, and Na). Because these particles were the first ones to form they are also called primary particles. These particles constitute the 0.1-µm (aerodynamic size) mode in mass size distributions and the 40–60-nm mode in the number size distributions. Examination of the detailed structure of these particles revealed that the primary particles that were seen as spherical in the SEM had even finer structures inside (Fig. 6, Paper B). The inner part of these particles consists of the nucleated gaseous metal oxide species (vaporised in the combustion) and the following layers are formed by the condensation of other fuel ash species and tar, soot etc., as observed by Burtscher et al. (1998) and Ishiguro et al. (1997). The inner core can also contain some soot. However, during the late combustion and early exhaust strokes a large part of the soot present in the fine mode oxidises and burns. Regardless of the soot burning the diesel exhaust particles may contain a lot of soot. Some sulphuric acid condensation on the surfaces may also occur.

The second main class of particles (coarse mode) consisted of cluster and catenulate aggregates, which are composed of the primary spherical particles found in the fine mode. The primary particles (approx. 50 nm in diameter) are adhered and partly sintered together to create cluster aggregates (Fig. 5b, Paper B). These types of aggregates were probably broken off from surfaces (re-entrained particles) after growing as a result of the deposition of small primary particles on to these surfaces. Aggregates indicating at least partial fusion of the primary particles and therefore the loss of their microstructure were also observed. Moreover, acicular structures demonstrating crystal growth were found. These particles constitute the large particle mode at about 10 μm (aerodynamic diameter) in the mass size distributions.

Other important distinguishable particle classes contributing to the coarse mode were the particles formed from the fuel oil droplet residue (Fig. 5c, Paper B) and the particles indicating mechanical abrasion (sharp-edged particles). The residue particles should contain the heavy elements of the fuel oil ash and some heavy carbon compounds after the volatilisation and burning of the fuel oil droplets. The conditions during the compression stroke in the cylinder are very favourable for soot formation (Heywood, 1989). The remaining fuel oil residue particles were typically almost spherical and about 0.1–0.6 μm in diameter. Some small particles were usually adhered and/or coagulated on the surface of these particles. Craters were also found on the surface of some of these particles, indicating some kind of chemical burst reaction (Fig. 5c, Paper B). These particles may make a significant contribution to the particles observed between the 0.1-μm and 10-μm modes in the mass size distributions (Fig. 4, Paper B).

4.1.4 Chemical composition of the particles

The exhaust ash aerosol relative elemental mass size distributions for Na, Ni, S, V, Ca, and Zn were determined with ICP-MS and ICP-AES analyses from the BLPI samples. The elemental mass size distributions were normalised in relation to the large engine at 50% load (base case) and were bimodal, similarly to the total mass size distributions, modes at about 0.1 and 10 μm (aerodynamic diameter; Fig. 7, Paper B). The distributions demonstrated that the only elements making a significant contribution to the 10-μm mode were sulphur and calcium. The large engine at 110% load and small engine 2 (relative size 0.1) at 100% load (same fuel oil) both had about the same amount of Ni and V under the 0.1-μm

mode. However, small engine 2 had much more Na under the 0.1-µm mode than the comparable large engine.

When dividing particles into two main classes, fine mode (≤ 0.4 µm, aerodynamic) and coarse mode (> 0.4 µm, aerodynamic), the 0.1-µm mode generally had over 70% of the elemental particle concentration, except for the large engine at 50% load (Table 6, Paper B). This suggested that the fuel oil ash was very highly volatile. Ca and Zn, though, were mainly present in the coarse mode, as the fractions were over 0.7. The main source for these elements, however, is the lubricating oil, which is not exposed to such high temperatures. Therefore, the Ca and Zn did not necessarily volatilise in any significant amounts.

SEM and EDS analyses were performed on the ash piles collected with the BLPI. The results for small engine 2 (relative size 0.1) at 100% load and HA-HFO from BLPI stages 3 (0.1-µm mode, aerodynamic diameter) and 10 (10-µm mode, aerodynamic diameter) indicated that carbon (42 wt. %) and oxygen (35 wt. %) made a major contribution to the 10-µm mode (Figure 1a). For the 0.1-µm mode the carbon content was 11% and oxygen 43 wt. %. The results suggested that there were fuel oil residue particles, unburned carbon, or heavy aromatics present, especially in the 10-µm mode. Moreover, some hydrocarbon condensation during sampling on to the surface of the 0.1-µm mode particles is possible. On the basis of the mass balances, only a very small fraction of the fed sulphur (about 1–3 wt. %) was found on the particles. This indicated that no severe sulphuric acid condensation occurred in these conditions (T > 150°C with simultaneous dilution of the sample flow).

The elemental concentrations determined by EDS from stages 3 and 10 of BLPI were also compared to the concentrations analysed with ICP-MS and ICP-AES (Figure 1b). As it is not possible to analyse carbon or oxygen with ICP techniques, these results were taken from the EDS analyses. Comparison of the elemental concentrations for stage 3 of BLPI (0.1-µm mode) for vanadium, sodium, and nickel, the main elements of the ash particles, with the EDS analyses indicated good comparability, except for nickel (Figures 1a and b). The concentration of nickel determined by EDS was only about 60% of the value analysed by ICP-MS. However, the concentrations determined by EDS were based on the average value of only eight single determinations, whereas the ICP results represent a bulk composition of the ash particles.

a)

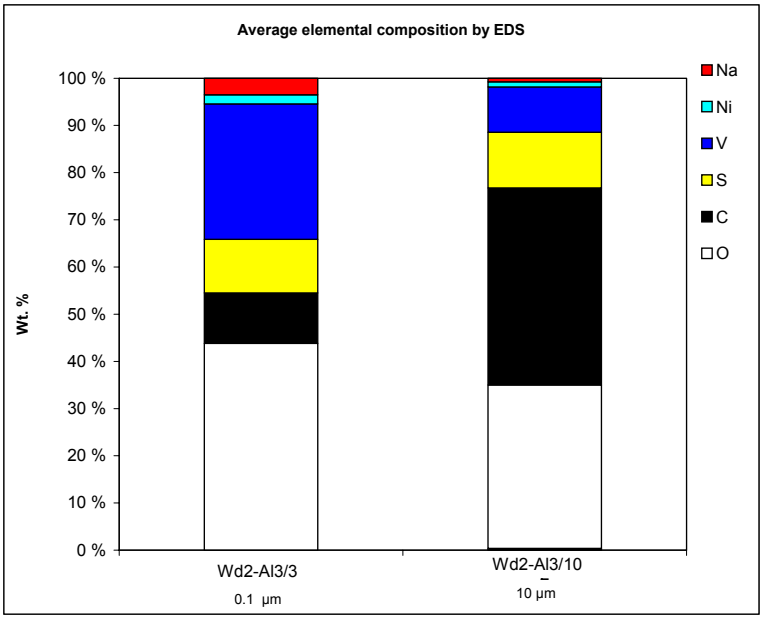

b)

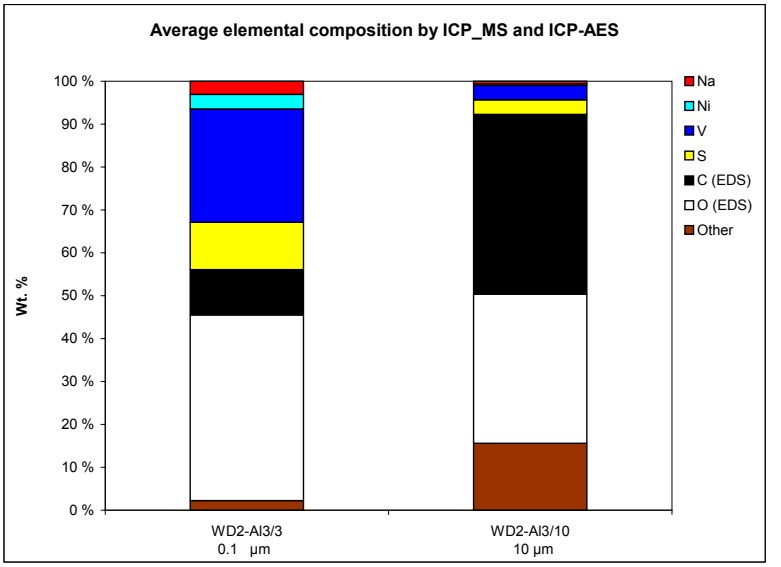

Figure 1. Elemental composition of the exhaust gas ash particles from BLPI stage 3, small particle mode (0.1 µm) and stage 10, large particle mode (10 µm) for small engine 2 (relative size 0.1). a) EDS b) ICP-MS and ICP-AES.

For stage 10 of BLPI (10-µm mode) the comparability between EDS and ICP-MS and ICP-AES was not so good (Figures 1a and b). This indicated that there was variation in the composition of these particles. Moreover, the concept of re-entrained particles also supports this finding. Because re-entrainment is a random process the history that these particles have undergone can vary considerably, depending on the time they have spent on the surfaces before re-entraining into the exhaust gas flow. Therefore, their composition and morphology may be far from homogeneous.

The chemical compounds constituting the exhaust ash particles were estimated on the basis of elemental concentration results by EDS and ICP-MS and ICP-AES from BLPI stages 3 (0.1-µm mode) and 10 (10-µm mode). The estimation was carried out by assuming that the most stable oxide of the elements forms, with the exception that all sodium forms Na_2SO_4. The remaining sulphur was assumed to form H_2SO_4. This estimation was based on an aerosol modelling calculations (ABC = Aerosol Behaviour in Combustion; Jokiniemi, et al., 1994). If there was still remaining oxygen after these calculations it was assumed to form moisture, i.e. water.

Comparison of the results with EDS and ICP for BLPI stage 3 (0.1-µm mode) for estimated chemical compounds (Figures 2a and b) gave very similar results, as expected from the comparison of the elemental composition analyses (Figures 1a and b). The mass balances based on the estimated chemical compound calculations were also good. The only difference was that in the case of ICP analyses the particles contained a small amount of moisture, about 1.5 wt. %. However, there was not enough oxygen in the particles to form vanadium pentoxide. Therefore, it was assumed that the rest of the vanadium is vanadium dioxide, which was also found to be formed on the basis of model calculations (Jokiniemi et al., 1996). Thus the particles were found to contain about 29 (27) and 20 (19) wt. % vanadium pentoxide and dioxide by EDS (ICP-MS) analyses, respectively. Of the total vanadium present in the particles 57 wt. % was in pentoxide form and 43 wt. % in dioxide form. The conditions in the engine and in the exhaust pipe at the measurement location (T = 340°C) are unfavourable towards the complete oxidation of vanadium into vanadium pentoxide. This can be caused by many different factors, such as short residence times or carbon containing particles acting as surface toxicants by blocking the active surface. However, the estimated amount of sulphuric acid in the particles was high, being

approx. 27 wt. %. This, on the other hand, requires the formation of vanadium pentoxide to catalyse the oxidation of SO_2 to SO_3 to form sulphuric acid.

For BLPI stage 10 (10-µm mode) the comparison of the results by EDS and ICP did not give such good results as expected from the comparison of the elemental composition analyses (Figures 2a and b). The main reason for this was the considerable lack of homogeneity of the particles, caused by re-entrainment. The 10-µm mode actually contained more sulphuric acid (34 wt. %) than the 0.1-µm on the basis of the EDS analyses. However, on the basis of the ICP-AES analyses, the 10-µm mode particles contained only about 9 wt. %. The moisture content, based on the estimated ICP results, was also high, being approx. 28 wt. %. This was, however, partly the consequence of the mass balances between the EDS and ICP elemental composition results not being so good.

a)

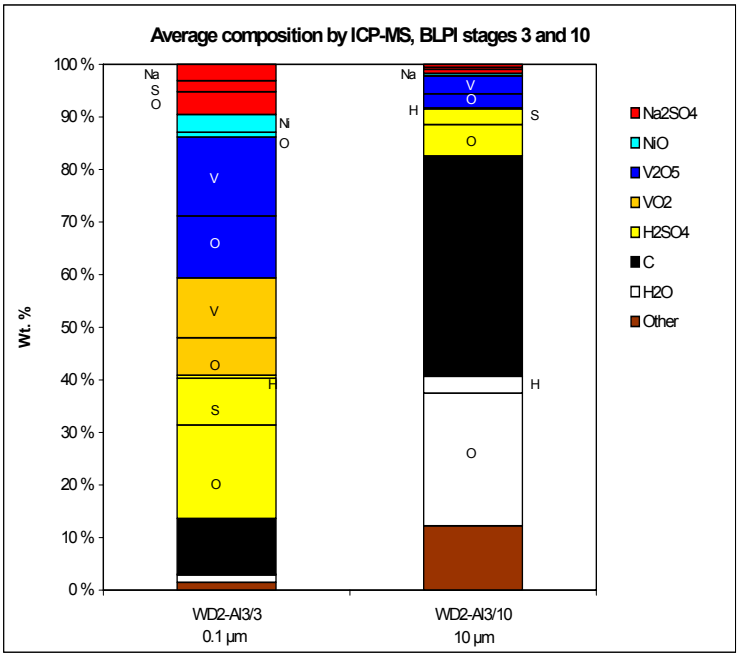

b)

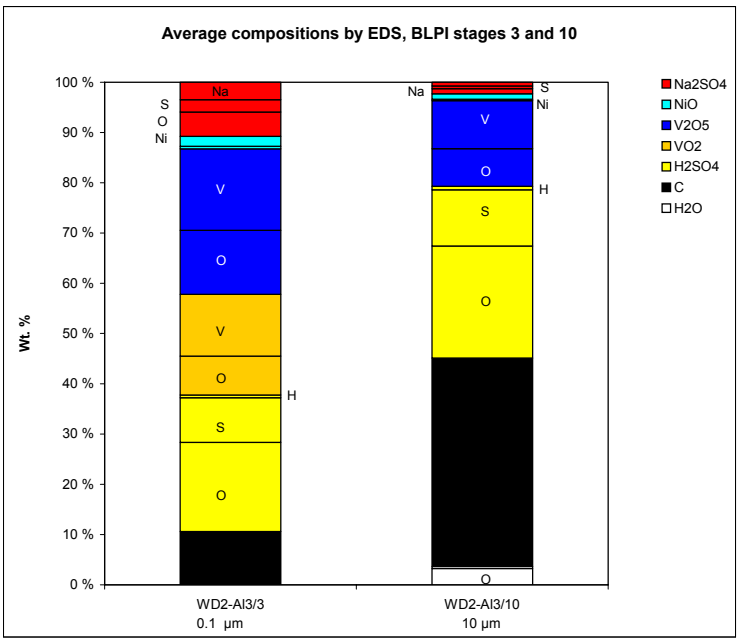

Figure 2. Estimated chemical compounds constituting the exhaust ash particles at BLPI stage 3, small particle mode (0.1 µm) and stage 10, large particle mode (10 µm) for small engine 2 (relative size 0.1). a) EDS b) ICP-MS and ICP-AES.

4.1.5 Effects of additives on particle characteristics

The effect of Mg-based fuel oil additives on the characteristics of exhaust gas ash particles was studied by operating a small auxiliary marine diesel engine (small engine 2, relative size 0.1) with HA-HFO. The mass concentrations with the additive were about 87–91% of the cases without any additive.

The exhaust ash aerosol mass size distributions in the size range 0.01–15 μm (aerodynamic size) were bimodal for the fuel oil without any additive and trimodal for the fuel oil with additive (Fig. 2, Paper C). The distributions were normalised in relation to the case of small engine 2 (1) without any additive. For the fuel oil with additive there was an additional mode at 2 μm, in addition to the modes at 0.1 μm and 10 μm (aerodynamic size).

The elemental mass size distributions for the without-additive case were bimodal, as noted before. However, in one case Ni, V, Na, and S made an important contribution to the 10-μm mode. For the additive cases the elemental mass size distributions were trimodal for Ni, S, and V in some cases. For Na and Mg the distributions were basically bimodal. The effect of the additive was clearly observed in the Mg relative elemental mass size distribution as a peak in the 2-μm mode (Fig. 6, Paper C).

With the fuel oil additive the particles seemed more spheroidal. In addition, more catenulate particles, rather than partly sintered ones, were observed. This could be the consequence of the Mg-based additive, which increased the melting point in the deposits and made re-entrainment easier and decreased the size of the re-entrained particles. Mg can also enhance the burnout of heavy aromatics, soot, carbon, etc. in the particles acting as a carbon oxidation accelerator (catalyst) and thus allows the particles only to agglomerate, but not to sinter. This carbon burnout is most effective for the 0.1-μm mode. Similar effects of fuel oil additives are also presented by others (Zhang and Megaridis, 1996; Kasper et al., 1999). In addition, Howard and Kausch (1980) report that two other possible soot oxidation mechanisms exist. In the first, the ionic mechanism (I; mainly alkaline metals), the additive ionises in the flame and the ions thus formed decrease the nucleation and coagulation rate. This results in a decrease in the amount of soot formed and/or a shift in the size distributions towards smaller particles. In the other mechanism (II; mainly alkaline earths) the additives react

homogeneously with the flame gases to produce hydroxyl radicals. These radicals can act as soot removers. On the basis of these statements and the experimental observations, a Mg-based additive seemed to function according to mechanism I, as the total concentration with the additive was clearly lower than without any additive and the 10-μm mode (or part of it) is possibly shifted towards the smaller size at 2 μm. However, soot reduction can also occur by the formation of hydroxyl radicals (mechanism II).

4.2 Particle deposition on exhaust valve seat face surfaces – full-scale modelling studies

Deposition is defined as a mass transfer from the gas-particle phase on to the surfaces of the considered system. Deposition can occur as particle or vapour deposition. The deposition mechanisms for particles present in the gas phase are direct impaction, turbulent impaction, thermophoresis, Brownian motion, and gravitation. Vapours can deposit by direct condensation or by chemisorption, i.e. by adsorption on to the surface followed by chemical reaction(s).

The deposition calculations were carried out with an aerosol model (aerosol behaviour in combustion, ABC; Jokiniemi et al., 1994). The flow was assumed to be a fully developed turbulent flow. The boundary layer of the momentum of the flow can then be divided into three parts: a turbulent zone, a buffer layer (turbulence gradually dies out), and a laminar sublayer (Fig. 1, Paper D).

The main issues to consider in particle deposition are the turbulence of the flow and the boundary layer of the particle concentration, consisting of the buffer layer and laminar sublayer. The turbulence of the flow will have an impact on all of the above-mentioned deposition mechanisms because it controls how great an amount of the particles will be able to penetrate the buffer layer. In turbulent impaction the turbulent eddies transport the particles through the buffer layer into the laminar sublayer. To be able to deposit on to the system surfaces the particles will have to penetrate through the laminar sublayer; this can occur if the particles have enough momentum from the turbulent flow. The mechanism is then called turbulent impaction. Other mechanisms (thermophoresis, Brownian motion, and gravitation) can also transport the particles on to the surfaces and these mechanisms can occur simultaneously. Thermophoresis is defined as the

movement of particles caused by the hot, more energetic gaseous molecules towards the gaseous molecules near the colder surface(s).

4.2.1 Mechanisms for deposition build-up

The mechanisms for deposition build-up on to the valve seat face were based on model calculations made for a small marine main engine (relative size 0.4) at 750 rpm (one crank axle cycle 80 ms, i.e. whole cycle 160 ms). The deposition was not very sensitive to the engine type in question; other assumptions made in the calculations (mainly fully developed plug flow and sticking probability 1) had a greater impact on the results. The effect of the non-homogeneous conditions prevailing in the diesel engine was taken into account by carrying out sensitivity calculations.

The deposition on to the seat face of the exhaust valve was mainly particle deposition, the mechanisms being turbulent impaction and thermophoresis (Table 3, Paper D). Turbulent impaction was significant for the large mode particles (mode at 10 μm) and thermophoresis for the small mode particles (mode at 0.08–0.1 μm). Because the effect of direct impaction on to the seat face of the valve was of minor importance, it was examined separately as a case of a bend in a pipe.

About 66% of the deposition was caused by the turbulent impaction and 34% by thermophoresis in the base case. In the case of a low V/Na proportion (change in the fuel composition), the fraction of turbulent impaction was largest, being about 75%. Turbulent impaction and thermophoresis were almost equal in the case of a half-open valve (change in the deposition rate). In the case of a bend in a pipe all deposition occurred as direct impaction.

4.2.2 Deposition rates

The total deposition of differently sized particles was obtained by multiplying their concentration and deposition velocity. The deposition velocity of the large mode (10-μm) particles caused by turbulent impaction was larger than the deposition velocity of the fine mode (0.1-μm) particles caused by

thermophoresis. In the base case the effect of turbulent impaction extended to particles only slightly under 1 μm in size and in the case of a half-open valve as far as 0.1-μm particles. The deposition velocities of the particles between 0.1 and 1 μm were thus combinations of turbulent impaction and thermophoresis. In the case of a bend in a pipe the effect of turbulent impaction extended even further, to particles of about 0.01 μm in size (Fig. 8, Paper D).

4.2.3 Deposition flake-off

Deposition flake-off and particle re-entrainment are the key causes of irregular shaped particles, which can also seen on the SEM micrographs. In this study, though, the cleavage and peeling of the deposits, mainly from the exhaust valve surfaces (also turbine blades), was not studied in detail. Some information concerning deposit flake-off can be obtained from the 10-μm mode present in the mass size distributions, as the appearance was more or less random. This could be explained by the cleavage of the deposit material and/or re-entrained particles from the surfaces of the combustion system.

There are several factors that may affect the cleavage of the deposit layer or the stickiness of the deposit, e.g. fuel composition (the amount of ash), fuel additives, the composition of the lubricating oil, the chemical environment of the elements, the materials (valve materials, hardfacings, turbine blade materials, etc.), system temperatures, and flow velocities. Another important factor is the carbon (C) present in various forms in the particles; because these particles deposit on the surfaces, and most probably the C present in the particles is burned off, heat is released. The released heat can also have an effect on the deposit stickiness because of the temperature increase, which facilitates melting/sintering phenomena. The chemical reaction(s) taking place in the deposit can also vary significantly, because the gas atmosphere surrounding the deposit may first be reducing and then convert to oxidising.

While all of these factors have an impact on the deposit stickiness, the main contribution probably comes from the composition of the fuel and lubricating oil, different materials, and process and material temperatures. These are the main parameters determining the melting/sintering tendency of the deposited particles. The effect of fuel oil composition on the composition, structure, and

stickiness of the deposit altered significantly when the high ash content fuel oil (HA-HFO) was doped with a Mg-Si-based fuel oil additive; the thickness of the deposit layers was about 1/10 of that obtained with HA-HFO only. The structure of the deposit was also more porous and clinker-like structures (cobble-stone) were more uncommon. The porous and brittle structure of the deposit contributed to the small amount of the deposit and the ease of cleavage.

The most critical variable in using fuel oil additives with HA-HFO fuel oils is the proportion of Mg-V and Si-Mg (Bryers, 1996; Cortes et al., 1990; Scott, 1977; Kukin, 1973). The Mg in the additive mainly serves as a replacement for the Na present in the fuel oils, converting the sodium vanadylvanadates that may possibly form into less sticky magnesium vanadates with a higher melting point, thus reducing the amount and the corrosiveness of the deposition.

4.3 Particle and deposit characteristics in laboratory-scale studies

Particle and deposit characteristics play an important role in studying corrosion and erosion phenomena in different combustion systems. To classify and determine the effects and mechanisms of the corrosion and erosion it is important to know the morphology, structure, and composition of the depositing particles and the deposit. Additionally, the chemical reactions taking place in the deposit layer need to be recognised in order to find out how the depositing particles start to react/transform into the actual deposit. In addition, the forming deposit may have crucial effects on the corrosion/erosion mechanisms; these mechanisms can be totally different if the deposit is missing from the surfaces under corrosive/erosive attack.

Because there was a need to study deposition and corrosion in relevant conditions and there was no suitable laboratory-scale equipment available, a new system was built, a deposition-corrosion apparatus (DCA). This device would simulate especially the formation of the exhaust ash particles and their deposition and corrosion in a similar manner as in large-scale engines when the exhaust valve starts to open.

4.3.1 Particle characteristics

Particle mass concentrations were measured with a BLPI after the porous tube diluter (PRD; Fig. 1, Paper E) with two different dilution temperatures, 150 and 25°C. Depending on the vibrating frequency of the aerosol generator the mass concentrations at 150°C with SO_2(g) and synthetic ash particles (SAP) were 572 and 937 mg/m^{3}n. However, when the dilution of the sample flow was carried out with unheated N_2(g) (T = 25°C) the total mass concentration almost doubled.

The mass size distributions in the size range 0.01–15 μm (aerodynamic) were unimodal at 1.4 μm in aerodynamic size (Fig. 3, Paper E), irrespective of the composition of the feed or the dilution gas temperature. However, there were more particles in the submicron mode when diluting with cold N_2(g). A clear rise in the mass size distributions commenced at about 0.2 μm in aerodynamic size. This, together with increased mass concentration, indicated the condensation of sulphuric acid on the surfaces of the particles.

Compared to the mass concentrations and size distributions measured in the large-scale engines, the synthetic ash particles (SAPs) produced had a mode at larger particles, 0.1 (Fig. 4, Paper B) versus 1.4 μm (Fig. 3, Paper E). The SAPs produced were selected to be larger in order to ensure adequate deposition and deposition rates.

Synthetic ash particle (SAP) morphology was not significantly affected by the different dilution temperatures. At 150°C, only some flat "pools" with no detailed structure were found (Fig. 5, Paper E). In some cases there were small, almost spherical particles in the middle of the "pool". Small, nano-sized (diameter approx. 70–90 nm) spherical particles were also observed. With cold dilution the structure and morphology of the particles was very similar (Fig. 6, Paper E). The concentration of the nano-sized spherical particles was higher. However, as the SEM sampler (point-to-plane ESP) could not be heated, the aerosol flow cooled down when it finally reached the collection point.

The elemental composition of the individual SAP with cold dilution for V varied from 8–26 wt. %; Na was almost constant at 1 wt. %, Ni was 0–5 wt. %, and S 12–23 wt. %, the rest being O (Fig. 8a, Paper E). A similar calculation base as in the case of full-scale exhaust ash particles was applied to estimate the chemical

compounds that formed. With these assumptions the particles contained, on average, 57 wt. % sulphuric acid and 17 wt. % moisture (Fig. 8b, Paper E). With that high amount of sulphur it is possible that the particles sulphate, forming vanadium sulphates. However, even in this case there is still so much sulphur left that the amount of sulphuric acid formed is 37–49 wt. %.

With hot dilution the composition of the particles was almost identical, excepting the fact that the portion of moisture can be smaller when the chemical compounds are being calculated. This was the consequence of the higher dilution gas temperature.

4.3.2 Deposit characteristics

The analyses of the deposited SAP, i.e. deposit piles (schematics of formation; Fig. 2, Paper E), were divided into three parts: base, middle, and top of the pile. This was performed to find out the possible differences in the morphology and composition of the piles as a function of the distance from the surface of the samples. Multiple analyses were carried out at all of these locations in order to attain some statistical confidence. Samples with different exposure times, 8 h and 144 h, were also analysed to find out if there are any changes in morphology and/or composition. The sample temperatures ranged from 700–750°C.

For the 8-h experiment the height of the deposit pile (needle) was about 800 µm (Fig. 10a, Paper E). At the deposit base (Fig 10b, Paper E), thin and sharp acicular crystals were observed. Rectangular and hexagonal crystals with slightly rounded edges were also found. Towards the middle of the deposit pile the number of rectangular and hexagonal crystals increased, compared to the number of acicular crystals. At the top of the deposit pile (Fig. 10d, Paper E), similar structures as in the deposit base were found. With the 144-h experiment there were indications of crystalline structures, but the sharp edges had disappeared. The crystals had also started to sinter/melt together, indicating partial sintering/fusion. This can be the consequence of the hot gas flow entering the fresh deposit. Therefore, the deposit that is building up can have a thermal insulation effect, especially near the surface of the sample slab. As a consequence, the deposit structure at the base, near the metal oxide layer, starts to crystallise. This thermal insulation effect of the deposits under boiler

conditions is well known, especially on the deposits found on heat exchanger tubes (Bryers, 1996). Sintering was also observed in the outermost layers.

The elemental composition for the 8-h experiment for V was in the range of 24–35 wt. %, irrespective of the location at the pile. For Ni the concentrations varied from 18–52 wt. % at the base, but levelled out clearly when advancing towards the middle and top of the pile, to 39–59 wt. %. The concentration of O was clearly lower at the base than in the middle or at the top of the pile. Therefore, the composition of the deposit pile did not change significantly when advancing from the middle of the deposit pile towards the top of the pile (Fig 13, Paper E).

With the 144-h experiment the elemental composition was, generally, similar to that found in the 8-h experiment. The major differences at the deposit base were a smaller Ni concentration, higher O concentration, and the presence of Cr (up to 3 wt. %). Advancing from the middle parts to the top of the deposit pile, the concentration of O increased and the concentrations of V and Ni decreased (Fig 14, Paper E).

Hardly any S was found in the deposit piles. Only small amounts of S (a few wt. %) were found in the vicinity of the base material at the deposit base in the case of the 144-h experiment. This indicated that S, as $SO_2(g)/SO_3(g)$, was transported through the deposit pile into the base material, Nimonic 80 A, where it reacted to form islands rich in S, Cr, and Ti, i.e. internal sulphidation precipitates, which contained up to 30 wt. % S (Figs. 5–6, Paper F). The S-content of these "islands" was in the same range as in the particles produced in the laboratory system. However, at some locations S and Na were found together. This simultaneous appearance of sodium and sulphur may indicate the presence of sodium sulphate.

4.4 Corrosion characteristics in laboratory-scale studies

A different corrosion research approach was selected here by designing a new experimental facility. With the deposition-corrosion apparatus (DCA) simulation of the formation of the exhaust ash particles, their deposition and corrosion occurs in the same way as in large-scale engines. Different materials were studied, but the results will concentrate on Nimonic 80 A (nominal composition,

Cr 20%, Fe 3.0%, Ti 2.4%, Al 1.4%, Si 1.0%, C 0.1%, and Ni as balance (wt. %)) as it is currently an industry standard material for large-scale diesel engines operating with problematic fuel oils. The sample temperatures ranged from 700–750°C.

The total deterioration caused by the deposited SAP and corrosion on the areas of the surface under the deposits were determined as a sum of the depth of a corrosion pit and the thickness of the bottom layer underneath the pit. The depth of the corrosion pit was defined by measuring the distance from the bottom of the pit to the deposit base in SEM. The thickness of the bottom layer was defined as the distance between the unattacked base material and the bottom of the corrosion pit (Figure 4). In this manner it was found that the total deteriorated area, i.e. pit + bottom layer, increased with temperature (26 μm at 700 and 87 μm at 750°C; Table 3, Paper F). There was no maximum at 700°C, as in the case when only the depth of the corrosion pit was considered.

4.4.1 Corrosion morphologies and chemical composition

Generally, advancing from the bottom of the pit towards the surface of the deposit, the structure was initially crystalline, but transformed near and at the surface of the pit into one that was more irregular and sintered/fused. The porosity also increased. This is caused by outward Cr lattice/grain boundary diffusion (Kofstad, 1988). From the interface between the pit and bottom reacted layer needles/pegs penetrating into the bottom reacted layer were seen (the "keying effect", Figs. 4d–e, Paper F). These pegs can serve as "anchors" for the deposit/oxide layer (Kofstad, 1988). Al was found at the vertexes of these pegs (Fig. 5, Paper F). This indicated that there was not enough Al to form a continuous aluminium oxide layer.

A zone of "black islands", i.e. indications of internal corrosion, (Figs. 4e and 5, Paper F) was discovered in the bottom layer under the pit. The size of these "black islands" varied, the smallest being under 0.5 μm and the largest about 3 μm in diameter. These islands contained 15–33 wt. % S, 8–38 wt. % Cr, 6–58 wt. % Ti, and 10–54 wt. % Ni (Figs. 5 and 6, Paper F). However, some of these islands consisted of 26 wt. % Cr, 37 wt. % Ti, and 26 wt. % O, with the

rest being V and Ni. These islands may be the “pre-existing” form of the oxygen-rich layer found in the pit area.

To analyse the samples in more detail, elemental corrosion profiles from rectangular areas on top of each other and covering the whole cross-section of the damaged area were performed. The results (Fig. 7, Paper F) indicated that generally Cr, Al, Ti, and Fe diffused from the base material (Nimonic 80 A) towards the surface of the pit. The highest Ti and Cr concentrations were observed at, or in the vicinity of, the bottom of the pit. The Cr concentration decreased almost steadily until it was almost zero near the deposit base, except for the case at 750°C, where Cr had propagated further in the deposit than in the other cases. Similar behaviour at 750°C was also observed for Ti. However, oxygen behaved differently in the high-temperature experiment at 750°C. In the 700°C experiments the oxygen concentration increased as the concentration of Ni and V decreased and vice versa. Vanadium, on the other hand, diffused strongly towards the base material, as it was found throughout the corrosion pit, although the relative concentration of V was much lower in the high-temperature 750°C case than in the 700°C case. S was not able to penetrate deeply into the pit or the bottom layer. On the other hand, distinct “black islands” rich in S were detected in the bottom layer (Figs. 4d–e and 5, Paper F).

4.4.2 Corrosion propagation

As no clear indications of totally melted/sintered deposits (no crystalline structure) were discovered, the fluxing mechanism responsible for the transport in melt deposits cannot be the sole explanation of the propagation of the corrosion. Therefore, other types of transport phenomena have to prevail.

Sulphur transport mode (atomic or molecular $SO_2(g)/SO_3(g)$ diffusion) into the deposit/base material was estimated by the method proposed by Stroosnijder and Quadakkers (1986a, b). For Nimonic 80 A under these conditions the only mode for sulphur transport was molecular $SO_2(g)/SO_3(g)$ diffusion. However, from the bottom of the deposit into the base material sulphur transport occurs by atomic sulphur diffusion via grain boundaries and/or by lattice diffusion. Grabke (1993) also considers sulphide formation, but in reducing conditions, and presents basically similar mechanisms for sulphur transport in metals/alloys.

In $SO_2(g)+O_2(g)$ environments it is necessary to consider the presence of $SO_3(g)$. Vanadium is known to (V_2O_5) catalyse the $SO_2(g)+O_2(g)$ oxidation reaction, the yield being heavily dependent on the gas atmosphere, adsorbing species, etc. (Dunn et al., 1998; Alvarez et al., 1999; Lapina et al., 1999; Alvarez et al., 2000). In adequate conditions the conversions can be as high as 80% in the presence of vanadium, but only a few per cent without vanadium. Because of the high amount of V present in the system as V_2O_5 (highly oxidising environment), $SO_2(g)$ can further react to $SO_3(g)$. $SO_3(g)$ is even more reactive than $SO_2(g)$ (Bryers, 1996). Therefore, with both $SO_2(g)$ and synthetic ash particles (SAP, including vanadium), more $SO_3(g)$ was formed and the corrosion rate was higher.

As the corrosion at 700°C was strongest with both $SO_2(g)$ and SAP feeds, the mutual effect of $SO_2(g)/SO_3(g)$ and SAP (vanadium) is critical. The Cr-based oxide layer in the pit area transformed into a more permeable form so that the diffusion over that layer was more rapid. Jones (1988), reports that sulphur can increase the activity of vanadium compounds (mainly V_2O_5) and therefore enhance corrosion by solid/gas transport promoted by a trace of V in the oxide lattice, and no liquid phase is present at the scale/base material interface (no fluxing of the elements). This would explain the faster corrosion found with both $SO_2(g)$ and SAP feeds, even though no severe indications of sintering were found.

The composition and size distribution of the particles produced and fed (SAP; Figs. 3 and 8, Paper E) also affected the phenomena occurring in the deposit and in the pit underneath. As reported in a model paper by Jokiniemi et al. (1996), the first particles formed by nucleation and were composed of NiO followed by sodium vanadates ($Na_2O{\cdot}V_2O_5$). Finally, vanadium oxide (VO_2) and Na_2SO_4 condensed on the surfaces of the nucleated particles. However, VO_2 probably oxidised further into V_2O_5. The composition of the particles indicated that the deposit contained, at least at the beginning, sodium sulphate. This was also confirmed by the 8-h experiment (1/01; Fig. 7a, Paper F), where the calculated Na/S ratios from the corrosion profiles were almost identical to the Na/S relation calculated for Na_2SO_4. In the other experiments (144-h), there was much more S at the same location as Na than compared to the composition required for the formation of Na_2SO_4. Therefore, the sulphur (as $SO_2(g)/SO_3(g)$) diffused through the porous deposit layer by molecular diffusion. When S, as $SO_2(g)/SO_3(g)$, reached the interface of the bottom layer depleted in Cr and base material, it reacted with Cr, which is the most stable oxide, and also with Ti and Ni to form

the internal sulphidation precipitates seen as “black islands” at the bottom layer. The “black islands” (Figs. 4d–e, Paper F), with both SO_2(g) and SAP feeds) were probably composed of a “mixed”-type sulphide ((Cr, Ti, Ni)S_x; Figs. 5 and 6, Paper F, elemental composition). However, the spatial resolution of the EDS is limited and the analysed locations (“black islands”) were in the Ni-concentrated metal matrix. Therefore, the amount of Ni might have been overestimated.

As there was hardly any O available in the bottom reacted layer these “black islands” may form by internal sulphidation. A similar kind of “sulphur front” corrosion is also reported by e.g. Jones and Williams (1987), Goebel et al. (1973), and Wright et al. (1993), who also presented a possible reaction path for scale development/internal sulphidation. Internal sulphidation via the grain boundaries is also possible (Narita and Ishikawa, 1987). As the oxide layer grows as a result of the lattice diffusion of oxygen (molecular O_2(g) diffusion is also possible in porous layers) inwards, more and more oxygen is available and the conditions become favourable for oxide formation (presumably (Cr, Ni, V, Ti)O_x “mixed” oxide/multiple oxide). In addition to the sulphur-rich “black islands”, only a few islands with no sulphur were found. The sulphur had been replaced by oxygen (26 wt. %), other elements being Cr (26 wt. %), and Ti (37 wt. %), with the rest being V and Ni. These islands may be the “pre-existing” form of the oxygen-rich layer found in the pit area. The sulphur-rich “black islands” may transform into these oxygen- and vanadium-containing islands as more and more oxygen diffuses into the bottom reacted layer where these islands are located and as the layer in the pit area grows. At this stage, however, there is not enough oxygen available for the formation of a continuous layer. When the layer in the pit area grows further, the chemical environment in the bottom layer changes (more oxygen available) and the sulphur from the “black islands” is released. The “oxide layer” (near the bottom of the pit) thus starts to grow and the released sulphur can then diffuse further in the base material by atomic sulphur diffusion and react to form a new front of “black islands”. Moreover, a strong oxygen concentration gradient existing over the formed oxide scale (pit area), and the inward diffusing SO_2/SO_3 coming into contact with the base material (metal) at the interface between the deposit base and base material, causes the SO_2/SO_3 to become instable. Thus it will dissociate to form atomic sulphur and oxygen molecule, and provides the sulphur needed for the internal sulphidation reaction (i.e. the formation of “black islands”).

To verify the suggested corrosion propagation model and to estimate the possibly forming chemical compounds, thermodynamical stability diagram calculations were performed. These diagrams, however, are only indicative in nature because it is assumed that a thermodynamical equilibrium between the phases under study is attained. The highly dynamical nature of the system also sets some requirements that a purely thermodymanical approach can not meet. It is possible that the conditions are locally very different ranging from highly oxidising at the surface of the deposit to reducing, e.g. between the deposit and the base material, even though the bulk atmosphere is highly oxidising. Therefore, the information gained by constructing these diagrams provides guidelines and limiting values for the possibly forming compounds/occurring reactions as no reaction kinetics is taken into account. With these limitations in mind, the thermodynamical stability diagrams indicate that the most stable oxides at the pit are Cr_2O_3 and V_2O_5, but nickel is in the form of $NiSO_4$ or $(NiO)(Cr_2O_3)$. The most stable oxide forms are highly dependent on partial pressures of sulphur dioxide and oxygen. However, these stability diagrams indicate, that the formation of the nickel chromates and sulphates (e.g. type II hot corrosion, also called “low temperature hot corrosion”; Kofstad, 1988) can not be entirely ruled out without further investigation with help of, e.g. XPS, XRD, from the pit area and bottom layer (Figure 4).

5. Conclusions

5.1 Particle characteristics on large-scale diesel engines

In large-scale, medium-speed (750–1000 rpm at 100% load) diesel engines operating with high ash content heavy fuel oils (HA-HFO; on the order of 0.1 wt. %) the prevailing conditions are very harsh during power stroke: temperatures approximately 2500°C and pressures 150 bar are common. Under these conditions nearly all ash and/or fuel oil species will volatilize. Therefore, the particles formed by the exhaust gas cooling via nucleation (ultrafine particles), condensation and/or chemical reactions contain a lot of the impurities of the fuel oil ash, mainly V, Na, and Ni. Moreover, the main additive components of the lubricating oil, Ca and Zn, volatilized in the cylinder during combustion may be found on the particles together with the fuel oil sulphur (on the order of 2.5 wt. %). The vapours formed in the cylinder (Na, SO_3(g), HCs, etc.) may condense heterogeneously on the surfaces of the existing ultrafine particles or condense homogeneously forming new particles, i.e. nucleate (Figure 3).

The exhaust ash aerosol relative mass size distributions in the size range of 0.01–15 μm (aerodynamic diameter) were, generally, bimodal. The main mass size mode (fine mode, 0.1-μm mode) was at 60–90 nm and a second mode at 7–10 μm in aerodynamic diameter (coarse mode, 10-μm mode). However, there were particles present through the whole size range. The 0.1-μm mode particles were 40–90 nm in physical diameter and almost spherical as analysed by electron microscope. These primary particles are generated by the nucleation of the gaseous fuel oil ash species and grow due to agglomeration and condensation. Soot, sulphuric acid, HCs and carbon can further form onto the surface of these primary particles thus leading into layer-like particle structures also seen by Ishiguro et al. (1997). The elemental composition of the particles analysed by EDS and ICP-MS (Figures 1a and b) also indicates that primary particles contain low amounts of carbon, < 10 wt. %. This further demonstrates that the small mode particles (primary particles, 0.1-μm mode) contain mainly fuel oil ash species. Furthermore, high amounts of metal oxide species further enhance carbon oxidation thus decreasing the amount carbon in the small mode (0.1-μm mode) particles.

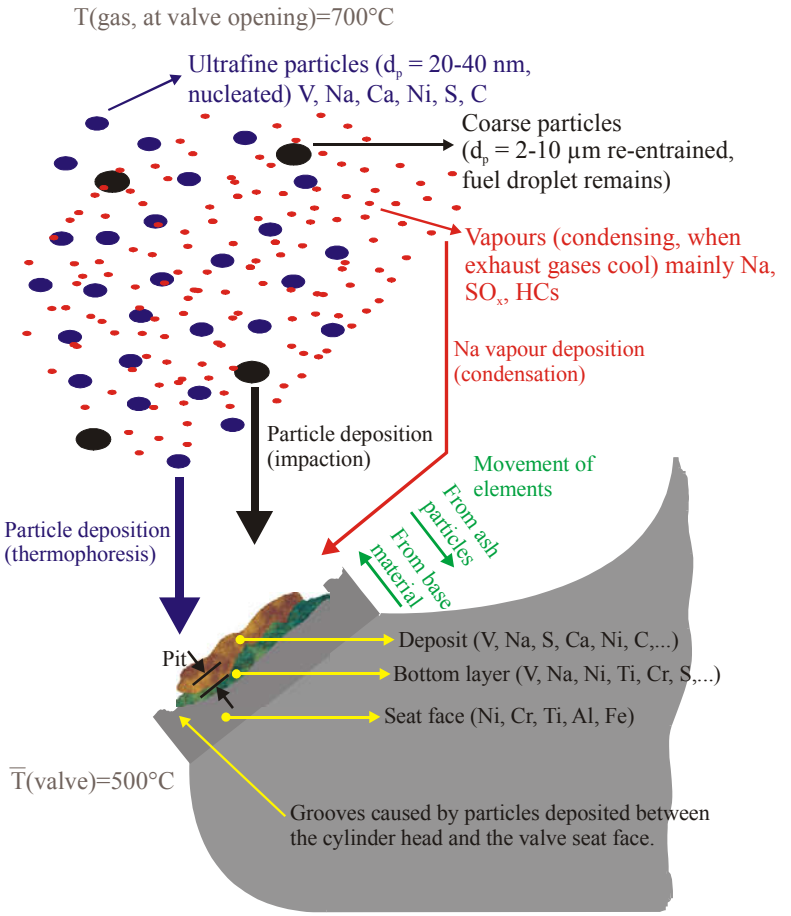

Figure 3. Simplified particle formation and deposition phenomena in large-scale diesel engines. Soot formation is not included (Papers B and C).

The large mode at about 10 µm in the mass size distributions was not observed in all of the process conditions studied. The particles in this mode resulted from incomplete combustion or the remains of the fuel oil droplets (unburnt carbon; physical size on the order of 200 nm). It is also possible that a fraction of this mode is produced by the re-entrained particles (physical size > 2 µm) from the surfaces of the combustion system (turbine blades, exhaust pipe surfaces, etc.). This would also be very plausible explanation considering that re-entrainment is a random process. The coarse mode (10-µm mode) particles consisted of cluster

and catenulate aggregates, which were composed of the primary particles. Agglomerates indicating partial fusion/coagulation and, therefore, losing their microstructure were also found. Large amounts of carbon (42 wt. %) and oxygen (35 wt. %) were found in the large mode particles. This suggested incomplete combustion in the engine. For the fine mode the corresponding contributions for oxygen and carbon are 43 wt. % and 11 wt. %, respectively (Paper B).

5.2 Deposition and corrosion characteristics on the laboratory scale

The mechanisms for deposition build-up on to the valve seat face were based on model calculations made for a small marine main engine (relative size 0.4) at 750 rpm. The deposition was not very sensitive to the engine type in question. The deposition on to the seat face of the exhaust valve was mainly particle deposition, the mechanisms being turbulent impaction for the large mode (10-μm) particles and thermophoresis for the fine mode (0.1-μm mode) particles. About 66% of the deposition was caused by the turbulent impaction and 34% by thermophoresis in the base case (i.e. normal operation conditions).

To simulate the flow passing the exhaust valve during the exhaust stroke of a large-scale diesel engine, a deposition-corrosion apparatus (DCA) was designed. The main particle deposition mechanism in this device was impaction caused by the very high velocity of the gas flow (about 100 m/s) that the synthetic ash particles (SAP; aerodynamic size 1–2 μm) fed into the system were not able to follow. The advantage of the DCA is that it simulates especially the formation of the exhaust ash particles and their deposition and corrosion in a similar manner as in large-scale diesel engines when the exhaust valve starts to open.

In the deposition-corrosion experiments carried out at temperatures 700 and 750°C, the composition of the particles indicated that the deposit contained, at least at the beginning, sodium sulphate. In the longer duration experiments, there was excess sulphur compared to that required for Na_2SO_4 formation. Therefore, the sulphur (as $SO_2(g)/SO_3(g)$) diffused through the porous deposit layer by molecular diffusion. When sulphur reached the interface of the bottom layer depleted in Cr and base material, it reacted with Cr, which is the most stable oxide, and also with Ti and Ni to form the internal sulphidation precipitates seen

as “black islands” at the bottom layer. The “black islands” with both SO_2 and synthetic ash particles feeds on were probably composed of a “mixed”-type sulphide, Cr, Ti, Ni)S_x. As there was hardly any O available in the bottom reacted layer these “black islands” may form by direct or grain boundary induced internal sulphidation. When the oxide layer grows inwards due to oxygen lattice diffusion or molecular oxygen diffusion (in porous layers), more and more oxygen is available and the conditions become favourable for oxide formation. Presumably “mixed” oxide/multiple oxide (Cr, Ni, V, Ti)O_x) are formed in this case.

In addition to the sulphur-rich “black islands”, only a few islands with no sulphur were found. In these islands sulphur had been replaced by oxygen. These islands may be the “pre-existing” form of the oxygen-rich layer found in the pit area. The sulphur-rich “black islands” may transform into these oxygen- and vanadium-containing islands as more and more oxygen diffuses into the bottom reacted layer and as the layer in the pit area grows. At this stage, however, there is not enough oxygen available for the formation of a continuous layer. When the layer in the pit area grows further, the chemical environment in the bottom layer changes (more oxygen available) and the sulphur from the “black islands” is released. The “oxide layer” (near the bottom of the pit) thus starts to grow and the released sulphur (in atomic form) can then diffuse further in the base material by atomic diffusion and react to form a new front of “black islands” (Figure 4). Moreover, a strong oxygen concentration gradient existing over the formed oxide scale (pit area), and the inward diffusing SO_2/SO_3 coming into contact with the base material (metal) at the interface between the deposit base and base material, causes the SO_2/SO_3 to become instable. Thus it will dissociate to form atomic sulphur and oxygen molecule, and provides the sulphur needed for the internal sulphidation reaction (i.e. the formation of “black islands”). In addition, based on calculations of thermodynamical stability diagrams the formation of the nickel chromates and sulphates (e.g. type II hot corrosion, also called “low temperature hot corrosion”; Kofstad, 1988) can not be entirely ruled out without further investigation with help of, e.g. XPS, XRD, from the pit area and bottom layer (Figure 4).

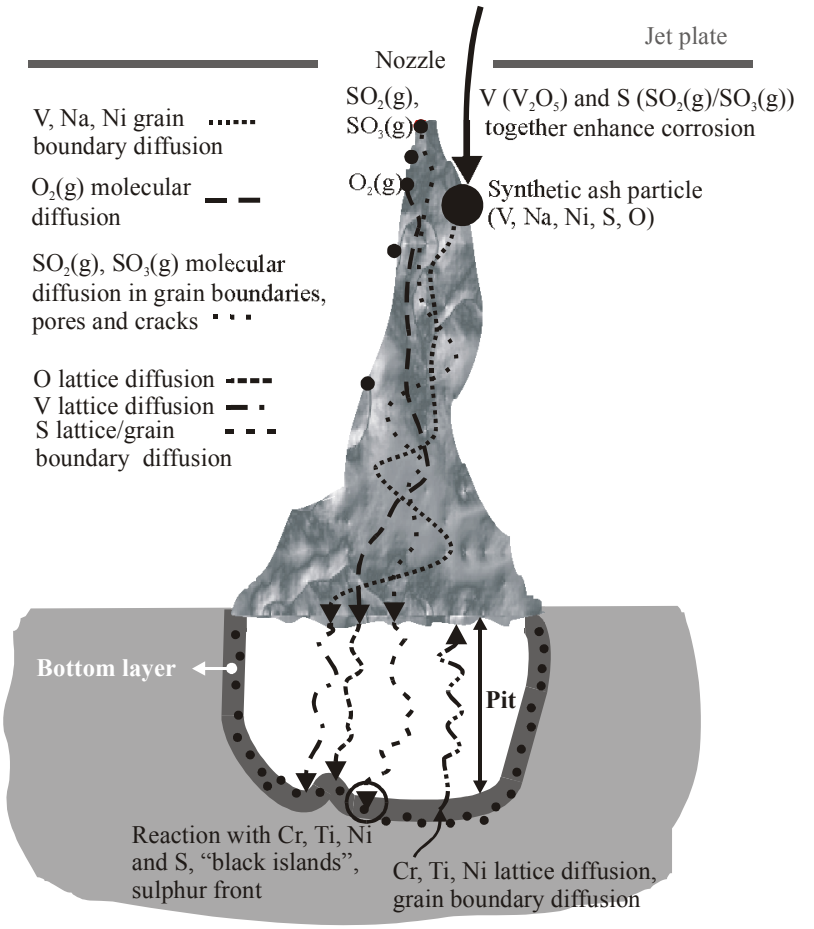

Figure 4. Corrosion propagation schematics for Nimonic 80 A material based on this study (Paper F).

To verify the experimental findings, an exhaust valve from a field endurance test 8600 h in duration was also analysed. A similar zone of sulphur-containing "black islands" was observed. As the temperature of the valve (T = 500°C) and oxygen content of the exhaust gas were different, the results are not directly comparable. However, the basic formation mechanism of these islands can still have similarities. The corrosion results with this experimental set-up are of the same order as those detected in large full-scale diesel engines under corresponding conditions (Schlager, 2001).

6. Recommendations for future work

Depending on the fuel oil the large-scale diesel is operated with, and whether it is a land-based power plant or marine vessel, the emission control technology applied is different. In marine applications catalysers (catalyst) and process optimisation (e.g. water injection) can usually provide good results in decreasing emissions. Currently, the health effects of light- and heavy-duty vehicles operating with relatively clean fuels are not well understood. Therefore, there have been, and are currently, many studies going on that deal with health-related issues concerning particles from different combustion sources (e.g. Wass, 2002; Pope et al., 2002; Lippmann, 2002; Donaldson et al., 1998; Morgan et al., 1997). Some years ago stationary large-scale diesel power plants were usually operated without any kind of after-treatment, i.e. emission control, devices. Therefore, future research on large-scale diesel engines will undoubtedly concentrate on decreasing emissions and on studying their health effects. As the health effects of particles depend on their size, shape, chemical composition, number, and mass, this will automatically direct interest towards the determination of particle characteristics and techniques for the control of particulate emissions. This usually means cutting down the amounts the amounts particles emitted, which is necessary as emission limits are becoming more and more stringent.

The sampling techniques, especially dilution techniques, are closely related to emission controls and health effects, because in almost every case when size distributions, especially those which are numerically based, or even concentrations, are being determined, dilution of the sample flow is a necessity. The optimum dilution system for the purposes of the experimental set-up depends greatly on the focus of the measurement. The aim may be to simulate the dilution effect when the exhaust gas enters the atmosphere and dilutes, i.e. to simulate atmospheric dilution. The target may also be to preserve the number size distributions in as unbiased a manner as possible from the measurement and dilution set-up artefacts and to produce an as-is size distribution of the exhaust gas as it would be observed inside the exhaust pipe. Both measurement methods are important, because the data from the as-is size distribution can be used to interpret the changes occurring in the atmospheric dilution. However, another possibility is to use only a single dilution system equipped with a device for volatilising the condensed and/or nucleated particles in one case and let them condense/nucleate in the other. Nevertheless, different dilution techniques need

experimental and modelling work in order for it to be possible to fully understand the best possible technique for each application and for the interpretation of the data. The most appropriate way to completely avoid "unwanted" nucleation/condensation is to keep the sample and dilution gas temperature together with the diluter temperature itself high enough.

For deposition and corrosion studies, more experimental and analytical work is needed in order to understand corrosion mechanisms in more detail. As an immediate further study for deposition-corrosion experiments, the separation of the Ni originating from the Nimonic 80 A sample alloy from the Ni originating from the produced synthetic ash particles would be interesting. This would give information on how far the Ni from the base metal can diffuse. However, this requires the use of e.g. tracer techniques.

For the determination of a more detailed corrosion mechanism, other analytical methods, such as XPS and XRD to define the chemical compounds, are very important. This is basically the only way to fully understand and to define the corrosion mechanism. Electrochemical methods can also provide valuable information on the possible mechanisms and kinetics. Therefore, the study of corrosion mechanisms has only been started by this research. Corrosion propagation schematics can be suggested by the results, but a more detailed mechanistic model requires more experimental and modelling work. However, the technique developed and applied here has proved to be suitable for producing adequate samples for the analyses. Furthermore, the benefit of this system is that particle formation and deposition occurs in a realistic way, as it does in full-scale engines.

References

Abdul-Khalek, I. S., Kittelson, D. B., Graskow, B. R., Wei, Q. and Brear, F. (1998) Diesel exhaust particle size: measurement issues and trends. *SAE paper 980525*, 133–145.

Abu-Qudais, M. and Kittelson, D. B. (1997) Experimental and theoretical study of particulate re-entrainment from the combustion chamber walls of a diesel engine. *Proc. Inst. Mech. Eng.* 211 D, 49–57.

Alvarez, E., Blanco, J., Avila, P. and Knapp, C. (1999) Activation of monolithic catalyst based on diatomaceous earth for sulphur dioxide oxidation. *Cat. Today* 53, 557–563.

Alvarez, E., Blanco, J., Knapp, C., Olivares, J. and Salvador, L. (2000) Pilot plant performance of a SO_2 to SO_3 oxidation catalyst for flue-gas conditioning. *Cat. Today* 59, 417–422.

Amann, C. A. and Siegla, D. C. (1982) Diesel particulates – what they are and why. *Aerosol Sci. Technol*. 1, 73–101.

Auvinen, A., Lehtinen, K. E. J., Enriquez, J., Jokiniemi, J. K. and Zilliacus, R. (2000) Vaporisation rates of CsOH and CsI conditions simulating severe nuclear accident. *J. Aerosol Sci.* 31, 1029–1043.

Baumgard, K. J. and Johnson, J. H. (1996) The effect of fuel and engine design on diesel exhaust particle size distributions. *SAE paper 960131*, 37–50.

Baxter, L., Miles, T. R., Miler Jr., T. R., Jenkins, B. M., Milne, T., Dayton, D., Bryers, R. W. and Oden, L. L. (1998) The behaviour of inorganic material in biomass-fired power boilers: field and laboratory experiences. *Fuel Processing Tech.* 54, 47–78.

Berner, A. and Lürzer, C. (1980) Mass size distribution of traffic aerosols in Vienna. *J. Phys. Chem.* 84, 2079–2083.

Berner, A., Lürzer, C., Pohl, F., Preining, O. and Wagner, P. (1979) The size distribution of the urban aerosol in Vienna. *Sci. Total Environment* 13 (3), 245–261.

Bonk, N. and Lange, J. (1994) Einflüsse von Kraftstoffskomponenten und motorischen Massnahmen auf die Abgaszusammentsetzung an einem schwerölbetribenen Schiffsdieselmotor. *Abgasemission von Schiffsdieselmotoren bei Schwerölbetrieb II (ASS II) 18 S 00117*, IFKO, Universität Hannover 149 p. (in German).

Brehob, D. D., Robben, F. and Saweyr, F. (1983) Performance of water emulsified residual fuels in a medium-speed diesel. *Am. Soc. Mech. Eng. paper 83-DGP-10*, 8 pp.

Bryers, R. W. (1996) Fireside slagging, fouling and high-temperature corrosion of hest-transfer surface due to impurities in steam-raising fuels. *Prog. Energy Combust. Sci.* 22, 29–120.

Burtscher, H. (1992) Measurement and characteristics of combustion aerosols with special consideration of photoelectric charging and charging by flame ions. *J. Aerosol Sci.* 23, 549–595.

Burtscher, H. (2005) Physical characterisation of particulate emissions from diesel engines: a review. *J. Aerosol Sci.* 36, 896–932.

Burtscher, H., Künzel, S. and Hüglin, C. (1998) Structure of particles in combustion engine exhaust. *J. Aerosol Sci.* 29, 389–396.

Burtscher, H., Matter, U. and Skillas, G. (1999) The effect of fuel additives on diesel engine particulate emissions. *J. Aerosol Sci.* 30 Suppl. 1, s851–s852.

Buseck, P., Cowley, J. and Eyring, L. (1992) High-resolution Transmission Electron Microscopy and Associated Techniques. New York: Oxford University Press. 645 p.

Cheng, Y.-S. (1993) Instrumental techniques/Condensation detection and diffusion size separation techniques. In: *Aerosol Measurement – Principles, techniques and applications* (Edited by Willeke, K. and Baron, P. A.). New York: Van Nostrand Reinhold. Pp. 427–451.

Concave product dossier no 98/109 (1998) Heavy fuel oils. *Concave product dossier no 98/109*, Brussels, Belgium 50 p.

Cooper, D. A. (2001) Exhaust emissions from high speed passenger ferries. *Atmos. Environ.* 35, 4189–4200.

Cooper, D. A., Peterson, K. and Simpson, D. (1996) Hydrocarbon, PAH and PCB emissions from ferries: a case study in the Skagerak-Kattegat-Öresund region. *Atmos. Environ.* 30, 2463–2473.

Cortes, V. J., Salvador-Martinez, L., Sanchez, E. J. and Plumed-Rubio, A. (1990) Particulate emission control in oil-fired boilers using in-oil magnesium oxide additives. In: *Proceedings: 1989 Fuel Oil Utilization Workshop* (Edited by Sanders, C. F., McDonald, B. L. and Miller, M. N.). Tustin, CA: Energy Systems Associates. Pp. 3.31–3.61.

Dolan, D. F., Kittelson, D. B. and Whitby, K. F. (1975) Measurement of diesel exhaust particle size distributions. *ASME paper 75-WA/APC-5*, 1–7.

Donaldson, K., Li, X. Y. and MacNee, W. (1998) Ultrafine (nanometre) particle mediated lung injury. *J. Aerosol Sci.* 29, 553–560.

Dunn, J. P., Korppula, P. R., Strenger, H. G. and Wachs, I. E. (1998) Oxidation of sulphur dioxide to sulphur trioxide over supported vanadia catalysts. *Applied Cat. B* 19, 103–117.

Fairbanks, J. W., Demaray, E. and Kvernes, I. (1984) Insulative, Wear and Corrosion Resistant Coatings for Diesel and Gas Turbine Engines. *Surface Engineering Conference: Surface Modification of Materials*, Les Arcs, France. Pp. 524–542.

Goebel, J. A., Petit, F. S. and Goward, G. W. (1973) Mechanisms for the hot corrosion of nickel-based alloys. *Met. Trans.* 4, 261–278.

Goldstein, J. I., Newbury, D. E., Ehlin, P., Joy, D. C., Romig Jr., A. D., Lyman, C. E., Fiori, C. and Lifshin, E. (1992) *Scanning Electron Microscopy and X-ray Microanalysis: A textbook for biologists, material scientists and geologists*. New York: Plenum Press. 820 p.

Grabke, H. J. (1993) Fundamental aspects of oxidation, sulfidation, chloridation and carburization in the gasifier environment. *Mat. High Temp.* 11 (1–4), 23–29.

Hall, E. L. (1992) Analytical electron microscopy. In: *Materials Science and Technology. A comprehensive treatment* (Edited by Cahn, R. W., Haasen, P. and Kramer, E. J.). *Characterisation of materials* (Edited by Lifshin, E.). 2A part I. Weinheim: VCH. Pp. 149–219.

Heywood, J. B. (1989) *Internal Combustion Engine Fundamentals*. New York: McGraw-Hill. 930 p.

Hillamo, R. E. and Kauppinen, E. I. (1991) On the performance of the Berner Low-Pressure Impactor. *Aerosol Sci. Technol.* 14, 33–47.

Hinds, W. C. (1999) *Aerosol Technology. Properties, behaviour and measurement of airborne particles.* New York: John Wiley & Sons Inc. 483 p.

Howard, J. B. and Kausch Jr., W. J. (1980) Soot control by fuel additives. *Prog. Energy Combust. Sci.* 6, 263–276.

Ishiguro, T., Takatori, T. and Akihama, K. (1997) Microstructure of diesel soot particles probed by electron microscope: first observation of inner core and outer shell. *Combust. Flame* 108, 231–234.

Iyer, K. J. L., Iyer, S. R. and Radhakrishnan, V. M. (1987) Hot corrosion cracking of Nimonic 80 A. *High Temp. Tech.* 5 (3), 145–150.

Jokiniemi, J. K., Lazaridis, M., Lehtinen, K. E. J. and Kauppinen, E. I. K. (1994) Numerical simulation of vapour-aerosol dynamics in combustion processes. *J. Aerosol Sci.* 25, 429–446.

Jokiniemi, J. K., Pyykönen, J., Lyyränen, J., Mikkanen, P. and Kauppinen, E. (1996) Modelling ash deposition during the combustion of low grade fuels. In: *Applications of Advanced Technology to Ash-related Problems in Boilers* (Edited by Baxter, L. and DeSollar, R.). New York: Plenum Press. Pp. 591–615.

Jones, R. L. (1988) Low-quality fuel problems with advanced engine materials. *High Temp. Tech.* 6 (4), 187–193.

Jones, R. L. and Williams, C. E. (1987) Hot corrosion of Co-Cr-Al-Y by molten sulfate-vanadate deposits. *Mat. Sci. Eng.* 87, 353–360.

Joy, D. C. (1992) Scanning electron microscopy. In: *Materials Science and Technology. A comprehensive treatment* (Edited by Cahn, R. W., Haasen, P. and Kramer, E. J.). *Characterisation of materials* (Edited by Lifshin, E.). 2A part I. Weinheim: VCH. Pp. 222–249.

Kasper, A., Aufdenblatten, S., Mohr, M., Forss, A., Matter, U. and Lutz, T. (2001) Particulate emissions from a marine diesel engine. *J. Aerosol Sci. Suppl.,* 32 S1, s79–s80.

Kasper, M., Sattler, K., Siegmann, K., Matter, U. and Siegmann, H. C. (1999) The influence of fuel additives on the formation of carbon during combustion. *J. Aerosol Sci*. 30, 217–225.

Kauppinen, E. I. (1992) On the determination of continuous submicrometer liquid aerosol size distributions with low-pressure impactors. *Aerosol Sci. Technol.* 16, 171–197.

Kerby, R. C. and Wilson, J. R. (1973) Solid-liquid phase equilibria for the ternary systems V_2O_5-Na_2O-Fe_2O_3, V_2O_5-Na_2O-Cr_2O_3, and V_2O_5-Na_2O-MgO. *Can J. Chem.* 51, 1032–1040.

Kerminen, V.-M., Mäkelä, T. E., Ojanen, C. H., Hillamo, R. E., Vilhunen, J. K., Rantanen, L., Havers, N., von Bohlen, A. and Klockow, D. (1997) Characterisation of the particulate phase in the exhaust from a diesel car. *Environ. Sci. Technol.* 31, 1883–1889.

Kittelson, D. B. (1998) Engines and nanoparticles: review. *J. Aerosol Sci.* 29, 575–588.

Kittelson, D. B. (1999) Personal communication.

Knutson, E. O. and Whitby, K. T. (1975) Aerosol classification by electric mobility: apparatus, theory and applications. *J. Aerosol Sci.* 6, 443–451.

Koch, W., Lodding, H. and Munzinger, F. (1988) Verdünnungsystem für die Messung hochkonzenrierter Aerosole mit optischen Partikelzähler. *Staub – Reinhaltung der Luft* 48, 341–344 (in German).

Kofstad, P. (1988) *High Temperature Corrosion.* New York: Elsevier Applied Science Publishers Ltd. 558 p.

Kukin, I. (1973) Additives can clean up oil-fired furnaces. *Environment. Sci. Technol* 7, 606–610.

Laskin, A. and Cowin, J. P. (2002) On deposition efficiency of point-to-plate electrostatic precipitator. *J. Aerosol Sci.* 33, 405–409.

Lapina, O. B., Balzhinimaev, B. S., Boghosian, S., Eriksen, K. M. and Fehrmann, R. (1999) Progress on the mechanistic understanding of SO_2 oxidation catalysts. *Cat today* 51, 469–479.

Lifshin, E. (1994) Electron microprobe analysis. In: *Materials Science and Technology. A comprehensive treatment* (Edited by Cahn, R. W., Haaen, P. and Kramer, E. J.). *Characterisation of materials* (Edited by Lifshin, E.). 2B part II. Weiheim: VCH. Pp. 353–421.

Lin, C.-Y. and Sheu, H.-R. (1997) Emissions from an oil-fired furnace burning MgO containing fuel oils. *J. Environ. Sci. Health* A32, 5, 1383–1392.

Lippman, M. (2002) Health effect of ambient air particles. *International Aerosol Conference 2002, Taipei, Taiwan*. Pp. 709–710. Available on CD.

Luthra, K. L. and Shores, D. A. (1980) Mechanism of Na_2SO_4 induced corrosion at 600–900 °C. *J. Electrochem. Soc.* 127 (10), 2202–2210.

Maricq, M. M., Chase, R. E. and Xu, N. (2001) A comparison of tailpipe, dilution tunnel, and wind tunnel data in measuring motor vehicle PM. *J. Air & Waste Management Assoc.* 51, 1529–1537.

Maricq, M. Matti, Podsiadlik, D. H. and Chase, R. E. (2000) Size distributions of motor vehicle exhaust PM: A comparison between ELPI and SMPS measurements. *Aerosol Sci. and Tech.* 33, 239–260.

Metcalfe, E. (1991) *Atomic Absorption and Emission Spectroscopy.* Chichester: John Wiley and Sons. 289 p.

Miller, C. A. and Srivastava, R. K. (2000) The combustion of Orimulsion and its generation of air pollutants. *Prog. Energy Combust. Sci.* 26, 131–160.

Mitchell, J. B. A. (1991) Smoke reduction from burning crude oil using ferrocene and its derivatives. *Combust. Flame* 86, 179–184.

Morgan, W. K. C., Reger, R. B. and Tucker, D. M. (1997) Health effects of diesel emissions. *Am. Occup. Hyg.* 41, 643–658.

Narita, T. and Ishikawa, T. (1987) Sulphidation properties of chromium and chromium-containing alloys at high temperatures. *Mat. Sci. Eng.* 87, 51–61.

Nicholls, J. R. (1993) Predicting the corrosion performance of alloys and coatings within diesel engines burning residual fuel oils. In: *Progress in the Understanding and Prevention of Corrosion*, Vol. 1. London: The Institute of Materials. Pp. 712–729.

Nicholls, J. R. (1994) Corrosion and wear resistance of some novel and current diesel exhaust valve materials. *Mat. High Temp.* 12 (1), 35–46.

Nicholls, J. R. and Stephenson, D. J. (1990) Hot corrosion tests on candidate diesel valve materials. *Trans. Inst. Marine Eng.* 102 (1), 47–60.

Nicholls, J. R. and Triner, D. A. (1990) The Influence of Fuel Composition on Lives of Current Valve Materials – Parametric Equations for Valve Life Prediction. *Inst. Marine Eng.* 102, 121–129.

Patashnick, H. and Rupprecht, G. (1986) Advances in microweighing technology. *Am. Lab.* 18, 57–60.

Patashnick, H. and Rupprecht, G. (1991) Continuous PM-10 measurements using the tapered element oscillating microbalance. *J. Air Pollution Control Assoc.* 41, 1079–1083.

Paro, D. (2001) Development of the sustainable engine. *Cimac 2001 Congress, Hamburg*. Pp. 263–271. Available on CD.

Pope III, C. A., Burnett, R. J. et al. (2002) Lung cancer, cardiopulmonary mortality, and long-term exposure to fine particulate air pollution. *J. Am. Med. Assoc.* 287, 1132–1141.

Rapp, R. A. (1987) Chemistry and electrochemistry of hot corrosion of metals. *Mat. Sci. Eng.* 87, 319–327.

Rapp, R. A. (2002) Hot corrosion of materials: a fluxing mechanism? *Corr. Sci.* 44, 209–221.

Rapp, R. A. and Zhang, Y. S. (1994) Hot corrosion of materials: fundamental studies. *JOM* December, 47–55.

Reynolds, T. and Pachaly, R. (1999) Technologies to optimise the operation and minimise emissions of heavy fuel oil fired boilers. In: *2nd International Colloquium on Fuels* (Edited by Bartz, W. J.). Ostfildern, Germany: Technische Akademie Esslingen, Weiterbildungzentrum. Pp. 441–452.

Rodriguez-Maroto, J. J., Sanz-Rivera, D., Dorronsoro, J. L., Gomez-Moreno, F. J., Muñoz-Bueno, R. and Martin-Espigares, M. (2001) Characterisation of particles emitted by a 14 MW low-speed diesel engine. *J. Aerosol Sci. Suppl.,* 32 S1, s77–s78.

Schlager, D. (2001) Personal communication.

Scott, J. F. (1977) Additive and fuel mixture to prevent corrosion and ash deposition in plants operated with fossil fuel. *German Patent 23 41 692*, App. 1973-08-17, Acc. 1976-06-10, 13 p. (in German).

Seiersten, M., Rätzer-Scheibe, H.-J. and Kofstad, P. (1987) Sodium vanadate induced corrosion of MCrAlY coatings – Burner rig studies. *Werkstoffe und Korrosion* 38, 532–540.

Shi, J. P. and Harrison, R. M. (1999) Investigation of ultrafine particle fromation during diesel exhaust dilution. *Environ. Sci. Technol.* 33, 3730–3736.

Shi, J. P., Harrison, R. M. and Brear, F. (1999) Particle size distribution from a modern heavy duty diesel engine. *Sci. Total Environ.* 235, 305–317.

Shi, J. P., Mark, D. and Harrison, R. M. (2000) Characterisation of particles from a current technology heavy-duty diesel engine. *Environ. Sci. Technol.* 34, 748–755.

Silvonen, A. (1996) 55% efficiency from diesel combined cycle (DCC). *Power News Wärtsilä Customer Journal* 3/96, 6–9.

Skillas, G., Qian, Z., Baltensperger, U., Matter, U. and Burtscher, H. (2000) The influence of additives on the size distribution and composition of particles produced by diesel engines. *Combust. Sci. and Tech.* 154, 259–273.

Srivastava, S. C. and Godiwalla, K. M. (1997) Review, Fuel ash corrosion of boiler and superheater tubes. *J. Materials Sci.* 32, 835–849.

Stroosnijder, M. F. and Quadakkers, W. J. (1986a) Review of high temperature corrosion of metals and alloys in sulphidizing/oxidizing environments II. Corrosion of alloys. *High Temp. Technol.* 4 (3), 141–151.

Stroosnijder, M. F. and Quadakkers, W. J. (1986b) Review of high temperature corrosion of metals and alloys in sulphidizing/oxidizing environments I. Corrosion of metals. *High Temp. Technol.* 4 (2), 83–96.

Tanner, S. C., Baranov, V. I. and Bandura, D. R. (2002) Reaction cell and collision cells for ICP-MS: a tutorial review. *Spectrochimica Acta* B 57, 1361–1452.

Umland, F. and Ritzkopf, M. (1975) Ventilkorrosion in Dieselmotoren. *Motortech. Z.* 36, 191–195 (in German).

Wass, U. (2002) Health Effects of Particulate Matter – What is Known and What Role is Played by Exhaust Particles? *Proceedings of the FISITA 2002 World Automotive Congress, Helsinki*, paper F02E333. 5 p.

Wright, I. G., Srinivasan, V. and Vedula, K. M. (1993) Some effects of minor alloying additions on the development and breakdown of the protective oxide scales. *Mat. High Temp.* 11 (1–4), 159–166.

Yeh, H.-C. (1993) Instrumental techniques/Electrical techniques. In: *Aerosol Measurement – Principles, techniques and applications* (Edited by Willeke, K. and Baron, P. A.). New York: Van Nostrand Reinhold. Pp. 410–426.

Zhang, J. and Megaridis, C. M. (1996) Soot suppression by ferrocene in laminar ethylene / air nonpremixed flames. *Combust. Flame* 105, 528–540.

Appendices of this publication are not included in the PDF version.
Please order the printed version to get the complete publication
(http://www.vtt.fi/inf/pdf/)

Published by

VTT

Series title, number and report code of publication

VTT Publications 598
VTT–PUBS–598

Author(s)
Lyyränen, Jussi

Title

Particle formation, deposition, and particle induced corrosion in large-scale medium-speed diesel engines

Abstract

The objective of this work was to study the formation of particles and their morphology and chemical composition in large-scale diesel engines operating with low-grade residual fuel oils. The effect of a Mg-based fuel oil additive on exhaust gas particles was also investigated. As particle and deposit formation and characteristics play an important role in corrosion and erosion, the particle characterisation studies provided the necessary background information.

The mass size distributions from the large-scale diesel engines were bimodal, with a main ("small") mode at 60–90 nm and a "large" mode at 7–10 µm. The small mode particles were formed by the nucleation of volatilised fuel oil ash species, which grew further by condensation and agglomeration. The large-mode particles were mainly agglomerates of different sizes consisting of small particles. These particles were re-entrained from deposits and fuel residue particles of different sizes.

Deposition and corrosion studies on the surfaces of the Nimonic 80 A sample slabs were carried out on a laboratory-scale with a newly set-up deposition-corrosion apparatus (DCA). A zone of "black islands" (15–33 wt. % S, the rest mainly Cr, Ni, and Ti) was found on the samples with SO_2(g) and synthetic ash particle (SAP) feeds. The composition of these islands suggested that they were composed of a "mixed"-type sulphide ((Cr, Ti, Ni)S_x). As there was hardly any O available in this bottom layer, the "black islands" were formed by internal sulphidation. A similar zone of sulphur-containing "black islands" was found on an exhaust valve from a field endurance test. However, based on calculations of thermodynamical stability diagrams the formation of the nickel chromates and sulphates (e.g. type II hot corrosion) can not be entirely ruled out without further investigation with help of, e.g. XPS, XRD, from the corrosion pit and the area underneath it.

Keywords

particles, particle formation, particle emissions, deposition, corrosion, internal combustion engines, medium-speed diesel engines, large-scale diesel engines, particle characteristics, laboratory-scale studies

ISBN

951–38–6708–0 (soft back ed.)
951–38–6831–1 (URL: http://www.vtt.fi/publications/index.jsp)

Series title and ISSN			Project number
VTT Publications 1235–0621 (soft back ed.) 1455–0849 (URL: http://www.vtt.fi/publications/index.jsp)			
Date April 2006	Language English, Finnish abstr.	Pages 72 p. + app. 123 p.	Price D

Commissioned by

Wärtsilä Ltd., Finnish Funding Agency for Technology and Innovation, VTT, Emil Aaltonen Foundation

Contact

VTT Technical Research Centre of Finland
Biologinkuja 7, P.O. Box 1000,
FI-02044 VTT, Finland
Phone internat. +358 20 722 111
Fax +358 20 722 7021

Sold by

VTT Technical Research Centre of Finland
P.O.Box 1000, FI-02044 VTT, Finland
Phone internat. +358 20 722 4404
Fax +358 20 722 4374

Julkaisija

Julkaisun sarja, numero ja raporttikoodi

VTT Publications 598
VTT–PUBS–598

Tekijä(t)
Lyyränen, Jussi

Nimeke

Hiukkasten muodostuminen, depositio ja hiukkasten aiheuttama korroosio suurissa, keskinopeissa dieselmoottoreissa

Tiivistelmä

Tässä työssä tutkittiin suurissa dieselmoottoreissa muodostuvia tuhkahiukkasia, niiden morfologiaa ja kemiallista koostumusta käytettäessä paljon tuhkaa (> 0,1 p.-%) sisältäviä jäännöspolttoaineita. Lisäksi tarkasteltiin Mg-pohjaisen lisäaineen vaikutusta tuhkahiukkasten muodostumiseen. Hiukkastutkimus loi myös välttämättömän pohjan hiukkasten deposoitumisen aiheuttamalle eroosio- ja korroosiotutkimukselle.

Suurten dieselmoottoreiden hiukkasmassakokojakaumat olivat kaksihuippuisia: päähuippu (pienet hiukkaset) oli 60–90 nm ja pieni huippu (isot hiukkaset) 7–10 µm kokoisissa hiukkasissa. Pienet hiukkaset muodostuivat polttoaineen haihtuvien tuhkaosaslajien ydintyessä, ja ne kasvoivat tiivistymällä ja liittymällä yhteen. Suuret hiukkaset koostuivat pääasiassa pienten hiukkasten muodostamista, erikokoisista yhteenliittyneistä hiukkasista. Nämä hiukkaset olivat depositioista irronneita ja/tai polttoainejäämistä muodostuneita hiukkasia.

Depositio- ja korroosiokokeet tehtiin itse suunnitellulla laboratoriomittakaavan depositio-korroosiolaitteistolla (DCA). Nimonic 80 A -materiaalin koekappaleissa havaittiin ”mustia saarekkeita” (15–33 p.-% S, loput pääosin Cr, Ni, ja Ti) käytettäessä SO2(g)-kaasua ja mallituhkahiukkasia (SAP) syöttönä. Näiden saarekkeiden koostumus viittasi niiden muodostavan ”sekasulfidin” ((Cr, Ti, Ni)Sx). Koska pohjakerroksessa hapen määrä oli hyvin alhainen, saarekkeet muodostuivat sisäisellä sulfidoinnilla. Samanlainen rikkipitoinen, ”mustista saarekkeista” muodostuva vyöhyke havaittiin kenttäkokeesta analysoidusta pakoventtiilistä. Kuitenkin termodynaamisten tasapainostabiilisuusdiagrammien perusteella nikkelikromaattien ja -sulfaattien (eli tyypin II kuumakorroosio) muodostumista ei täysin voi sulkea pois ilman lisätutkimuksia esim. XPS:n ja XRD:n avulla.

Avainsanat

particles, particle formation, particle emissions, deposition, corrosion, internal combustion engines, medium-speed diesel engines, large-scale diesel engines, particle characteristics, laboratory-scale studies

ISBN
951–38–6708–0 (nid.)
951–38–6831–1 (URL: http://www.vtt.fi/publications/index.jsp)

Avainnimeke ja ISSN			Projektinumero
VTT Publications 1235–0621 (nid.) 1455–0849 (URL: http://www.vtt.fi/publications/index.jsp)			
Julkaisuaika Huhtikuu 2006	Kieli Englanti, suom. tiiv.	Sivuja 72 s. + liitt. 123 s.	Hinta D
Projektin nimi		Toimeksiantaja(t) Wärtsilä Oyj, Tekes, VTT, Emil Aaltosen Säätiö	

Yhteystiedot

VTT
Biologinkuja 7, PL 1000, 02044 VTT
Puh. vaihde 020 722 111
Faksi 020 722 7021

Myynti

VTT
PL 1000, 02044 VTT
Puh. 020 722 4404
Faksi 020 722 4374

The demands for higher efficiency in power-plant type diesel engines require an increase of the combustion temperatures. The aim is to extract the additional energy stored in hotter exhaust gases by installing a secondary steam turbine in the exhaust pipe, and efficiencies on the order of 50% are achievable. However, reduction of lubrication and cooling in the cylinder and cylinder head are required, which means even higher temperature loads to materials. In addition, the engines are usually operated with low-grade residual fuel oils with high ash content. In this work particle formation mechanisms, characteristics, morphology and composition in large-scale diesel engines are studied. These studies provided the necessary background information for laboratory-scale deposition and corrosion research, based of which a corrosion propagation model is presented.

Tätä julkaisua myy

VTT
PL 1000
02044 VTT
Puh. 020 722 4404
Faksi 020 722 4374

Denna publikation säljs av

VTT
PB 1000
02044 VTT
Tel. 020 722 4404
Fax 020 722 4374

This publication is available from

VTT
P.O. Box 1000
FI-02044 VTT, Finland
Phone internat. +358 20 722 4404
Fax +358 20 722 4374

ISBN 951-38-6708-0 (soft back ed.)
ISSN 1235-0621 (soft back ed.)

ISBN 951-38-6831-1 (URL: http://www.vtt.fi/inf/pdf/)
ISSN 1455-0849 (URL: http://www.vtt.fi/inf/pdf/)